Cell Reports

The histone chaperone ANP32B regulates chromatin incorporation of the atypical human histone variant macroH2A

Graphical abstract

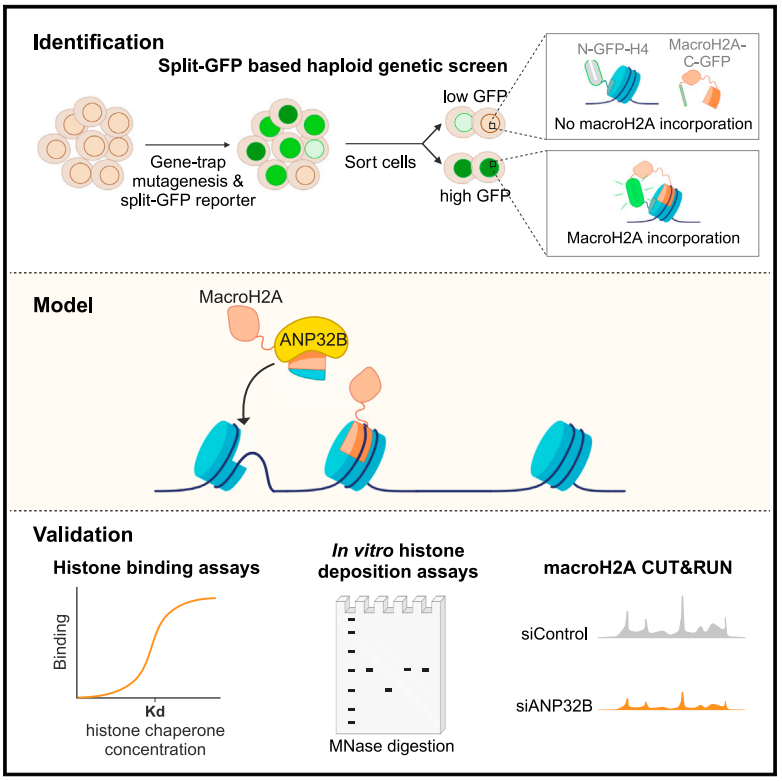

Highlights

- Split-GFP can be used as a high-throughput readout for chromatin incorporation
- Genetic screen identified macroH2A regulators
- ANP32B binds macroH2A-H2B dimers and deposits them onto tetrasomes *in vitro*
- Loss of ANP32B affects macroH2A chromatin localization on a genome wide scale

Authors

Imke K. Mandemaker, Evelyn Fessler, David Corujo, ..., Lucas T. Jae, Francesca Mattiroli, Andreas G. Ladurner

Correspondence

i.mandemaker@hubrecht.eu (I.K.M.), f.mattiroli@hubrecht.eu (F.M.), andreas.ladurner@bmc.med.lmu.de (A.G.L.)

In brief

Mandemaker et al. establish a split-GFP based assay to measure chromatin incorporation and use it to perform a genetic screen to identify regulators of the histone variant macroH2A. They show that ANP32B can directly bind to macroH2A and affect its deposition both *in vitro* and in cells.

Mandemaker et al., 2023, Cell Reports *42*, 113300
October 31, 2023
https://doi.org/10.1016/j.celrep.2023.113300

CellPress

Cell Reports

CellPress
OPEN ACCESS

Report

The histone chaperone ANP32B regulates chromatin incorporation of the atypical human histone variant macroH2A

Imke K. Mandemaker,[1,2,*] Evelyn Fessler,[3] David Corujo,[4,5] Christiane Kotthoff,[1] Andreas Wegerer,[1] Clément Rouillon,[2] Marcus Buschbeck,[4,5] Lucas T. Jae,[3] Francesca Mattiroli,[2,*] and Andreas G. Ladurner[1,6,7,*]

[1]Biomedical Center (BMC), Department of Physiological Chemistry, Faculty of Medicine, LMU Munich, 82152 Planegg-Martinsried, Germany
[2]Hubrecht Institute, Uppsalalaan 8, 3584CT Utrecht, the Netherlands
[3]Gene Center and Department of Biochemistry, LMU Munich, 81377 Munich, Germany
[4]Applied Epigenetics Program, Myeloid Neoplasm Program, Josep Carreras Leukaemia Research Institute (IJC), Campus ICO-GTP-UAB, 08916 Badalona, Barcelona, Spain
[5]Germans Trias I Pujol Research Institute (IGTP), 08916 Badalona, Barcelona, Spain
[6]Eisbach Bio GmbH, 82152 Planegg-Martinsried, Germany
[7]Lead contact
*Correspondence: i.mandemaker@hubrecht.eu (I.K.M.), f.mattiroli@hubrecht.eu (F.M.), andreas.ladurner@bmc.med.lmu.de (A.G.L.)
https://doi.org/10.1016/j.celrep.2023.113300

SUMMARY

All vertebrate genomes encode for three large histone H2A variants that have an additional metabolite-binding globular macrodomain module, macroH2A. MacroH2A variants impact heterochromatin organization and transcription regulation and establish a barrier for cellular reprogramming. However, the mechanisms of how macroH2A is incorporated into chromatin and the identity of any chaperones required for histone deposition remain elusive. Here, we develop a split-GFP-based assay for chromatin incorporation and use it to conduct a genome-wide mutagenesis screen in haploid human cells to identify proteins that regulate macroH2A dynamics. We show that the histone chaperone ANP32B is a regulator of macroH2A deposition. ANP32B associates with macroH2A in cells and *in vitro* binds to histones with low nanomolar affinity. *In vitro* nucleosome assembly assays show that ANP32B stimulates deposition of macroH2A-H2B and not of H2A-H2B onto tetrasomes. In cells, depletion of ANP32B strongly affects global macroH2A chromatin incorporation, revealing ANP32B as a macroH2A histone chaperone.

INTRODUCTION

Histones are at the core of packing DNA into chromatin. The main building blocks of chromatin are the nucleosomes, repeats of about 147 bp of DNA that are wrapped around octamers of histone proteins.[1] These canonical histones can be replaced by histone variants which may change the biochemical properties of the nucleosome and can carry specific post-translational modifications or recruit specific proteins.[2]

The most divergent histone variant is macroH2A. Besides the histone fold, macroH2A isoforms contain an additional 25-kDa globular domain called the macrodomain. Macrodomains have the ability to bind to NAD^+ metabolites,[3] and the macroH2A1.1 isoform binds ADP-ribose,[4] giving it functions in DNA damage repair[5,6] and PARP-1-mediated transcription.[7] In contrast, the ligands and biological function(s) of the macrodomains for the other two macroH2A isoforms (macroH2A1.2 and macroH2A2) remain unknown. A structural change in the L1 loop of the histone fold of macroH2A stabilizes nucleosomes,[8,9] and the linker connecting the histone fold with the macrodomain promotes chromatin compaction.[10] Therefore, it is not surprising that macroH2A is generally, although not exclusively, associated with transcriptional silencing[11–13] and is enriched in heterochromatin,[13,14] as well as on the inactive X chromosome.[15–17] Interestingly, macroH2A is important to maintain gene silencing in differentiated cell states and provides a barrier to cellular reprogramming.[18]

The chromatin incorporation and removal of histone variants is typically promoted and regulated by specific histone chaperones or adenosine triphosphate (ATP)-dependent chromatin remodelers. MacroH2A has been shown to be removed from actively transcribed regions by the chaperone complex FACT (facilitates chromatin transcription),[19] while ATRX negatively regulates its presence on telomeres and the α-globulin locus.[20] Recently, Hells/LSH (lymphoid-specific helicase) was also identified as a factor that affects macroH2A deposition. Loss of Hells resulted in a 40% reduction of chromatin-bound macroH2A,[21,22] indicating that there likely are more players involved in this process.

Here we developed a cellular assay that reports on the incorporation of a macroH2A histone into chromatin and then exploited the power of haploid cell functional genomics to reveal key regulators

of macroH2A incorporation. We found that acidic nuclear phosphoprotein 32B (ANP32B) affects macroH2A deposition. ANP32B belongs to the ANP32 family and, together with ANP32A, it is essential for the replication of the influenza virus within human cells.[23] Its homolog ANP32E is a histone chaperone for H2A.Z,[24] and ANP32B is also described to have histone chaperone activity.[25,26] This activity is associated with transcriptional silencing,[26] but so far, its exact role on chromatin as well as histone variant specificity was not well characterized. We show that ANP32B can directly bind macroH2A-H2B dimers and has the ability to deposit these dimers onto tetrasomes *in vitro*. Moreover, we show that ANP32B depletion affects macroH2A chromatin association in cells, indicating it is a macroH2A chaperone.

RESULTS

Split-GFP system as a high-throughput readout of macroH2A chromatin incorporation

To be able to identify regulators involved in macroH2A deposition using a genetic screening approach, we developed a high-throughput readout of macroH2A chromatin incorporation. For this, we exploited the split-GFP system, which enables us to assess whether two proteins are in close proximity.[27] Tagging histone H4 and macroH2A with complementary parts of the GFP molecule allows us to analyze whether the two histones are close by, because of the generation of the fluorescent signal (Figure 1A). As histone proteins are stable proteins, we constitutively expressed N-GFP1-10-H4, but placed macroH2A-C-GFP11 under an inducible promoter to ensure we study the effects on *de novo* macroH2A deposition only. In addition, we reasoned that a short expression time will prevent transcription and replication stress that may occur upon the possible stabilization of nucleosomes by the strong interaction between the two parts of GFP.

To test whether this split-GFP fluorescent readout can be used to analyze histone deposition, we generated split-GFP T-Rex 293 cells for two macroH2A isoforms, as well as for canonical H2A, containing N-GFP1-10-H4 and a C-GFP11-tagged (macro)H2A isoform (Figures S1A and S1B). Expression of the constructs was equal (macroH2A) or lower (H2A, H4) than endogenous histones levels. Fluorescence was only observed in these cells once doxycycline was added to induce the C-GFP11-tagged H2A or macroH2A isoforms. The GFP signal showed an overlap with Hoechst staining of pre-extracted cells, indicating the tagged histones are indeed present on chromatin (Figure S1A). Also, both macroH2A isoforms showed enrichment at bright DAPI-rich spots inside the nucleus, corresponding with the inactive X chromosome, indicating that localization of the histones is not affected by overexpression and tagging. Furthermore, we confirmed a doxycycline-dependent GFP signal within low-salt extracted samples from MNase digested split-GFP cells, which are highly enriched in mono- and di-nucleosomes (Figures 1B and S1C). To further validate the split-GFP system, we performed small interfering RNA-mediated knockdown of Hells in macroH2A1.1 split-GFP cells. In line with the known impact of Hells on macroH2A deposition,[21,22] we observed a significant decrease in GFP levels upon Hells depletion (Figures 1C and S1D). Together, this shows that our split-GFP assay is a suitable system to measure histone deposition in cells.

Haploid genetics screen identifies regulators of macroH2A deposition

To identify macroH2A regulators, we decided to use our split-GFP system in combination with a gene-trap screening approach. For this, we generated haploid cells with the macroH2A1.2 split-GFP system (Figures 1D, 1E, and S1E). We added an additional T2A-mCherry to the expression construct to ensure that any observed effects were caused by mutation of genes that affected the incorporation, but not the expression, of macroH2A-C-GFP11. In other words, we wanted to ensure that the screen picked up actual macroH2A regulators and not regulators of the TetON system that was used to express macroH2A-C-GFP11. These split-GFP HAP1 cells were used for gene-trap mutagenesis, and after 16 h of doxycycline treatment we sorted cells with the 5% highest and lowest GFP levels from the mCherry-positive population (Figures 1F and S1F). Next, we retrieved the gene-trap integration sites in these populations by deep sequencing. This identified several factors that impact macroH2A incorporation (Table S1).

Among the identified genes, we found that ATRX mutation led to increased GFP signal (Figure 1G). This is in accordance with its previously described negative effect on macroH2A incorporation at telomeres[20] and validated our cell-based functional genomics approach. Interestingly, we found that Hells was not a significant hit (ratio high/low GFP 1.11) in our screen, which could suggest cell- or isoform-specific roles for this chromatin remodeler in macroH2A dynamics. As the other known macroH2A regulator, the FACT complex is essential, and it is, therefore, inherently impossible to be picked up in such a screen. Moreover, we identified several components of the polycomb repressive complex 2 (PRC2) as significant genes whose mutation resulted in increased macroH2A deposition (Figure 1G). MacroH2A is enriched at H3K27me3 regions, interacts with PRC2, and stimulates its recruitment to the LOX locus.[13,28] Our screening results indicate that loss of the PRC2 complex resulted in increased macroH2A chromatin incorporation. Interestingly, experiments in the macroH2A1.2 T-Rex split-GFP cells using UNC1999, a small molecule inhibitor of the catalytic subunit of the PRC2 complex EZH2, confirmed that PRC2 activity affects the levels of macroH2A chromatin incorporation (Figures 1H and S1G). Overall, our assay thus validated a functional role for both ATRX and the PRC2 complex in macroH2A chromatin dynamics, indicating the potential of our unbiased haploid genetic screening approach in identifying important chromatin regulators.

Proteomics and genomic screens identify ANP32B as a potential macroH2A regulator

Our first priority in dissecting the data from the split-GFP-based genome-wide screen was aimed at identifying a histone chaperone for macroH2A deposition. The screen reveals direct as well as indirect regulators of macroH2A chromatin incorporation. To find the direct effectors, we performed pulldown experiments with recombinant His-macroH2A1.2-H2B dimers in HeLa cell extracts followed by mass spectrometry to find interactors (Figure 1I; Table S2). As expected, several histone chaperones were pulled down along with the His-macroH2A1.2-H2B dimers. However, only ANP32B was also identified as a significant hit in the genetic screen (Figure 1I), indicating a link between this protein in

CellPress
OPEN ACCESS

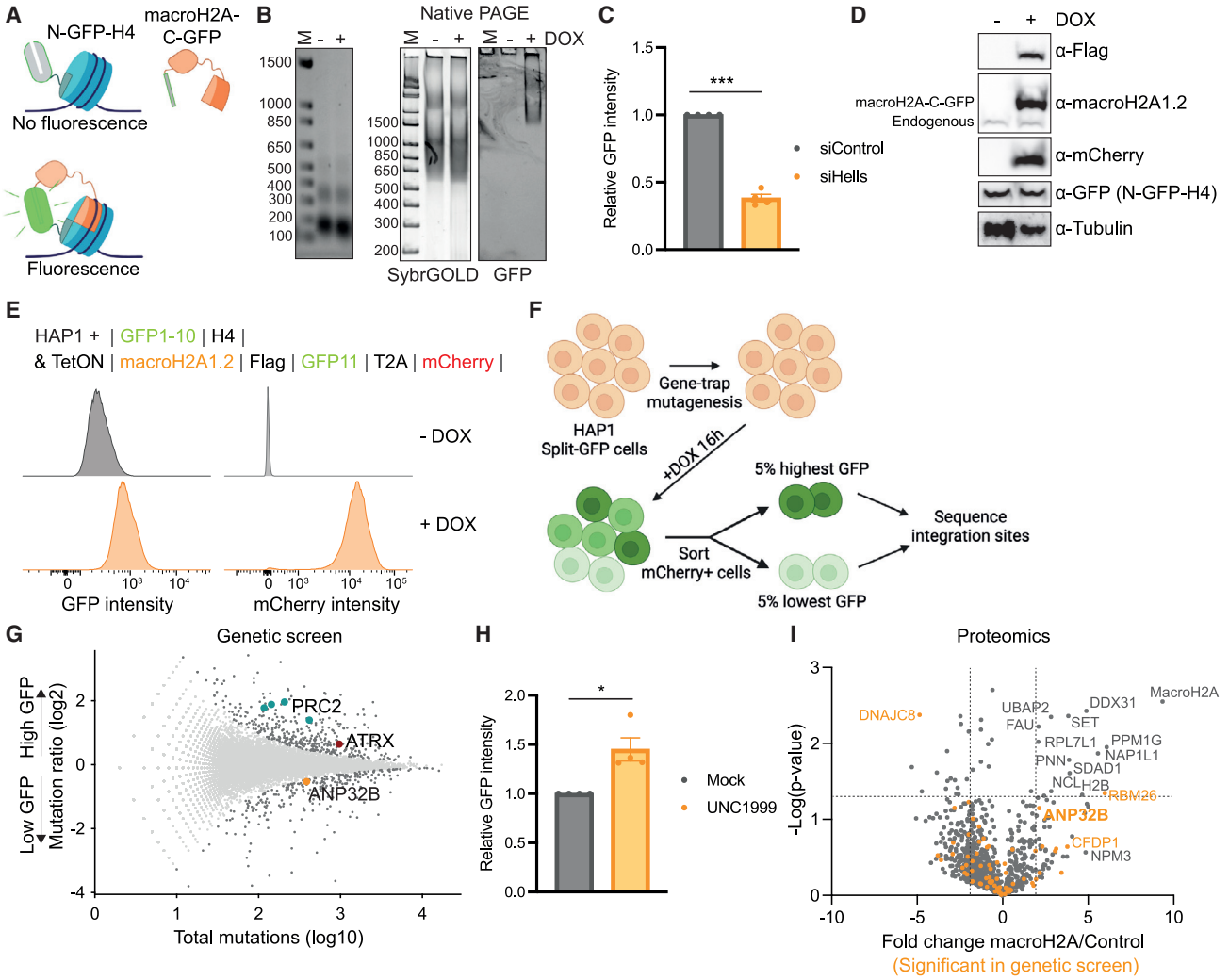

Figure 1. Genetic screen combined with proteomics identifies ANP32B as a potential regulator of macroH2A deposition

(A) Graphical representation of the split-GFP-based approach to measure macroH2A deposition onto chromatin. Created with BioRender.com.

(B) Nucleosomes from MNase-digested split-GFP cells with or without treatment with 1 μg/mL doxycycline (DOX) for 20 h visualized by denaturing agarose gel (left) or native PAGE (middle and right). Native PAGE was scanned for GFP signal before SYBR Gold staining to visualize DNA.

(C) Relative GFP intensity in control and Hells-depleted macroH2A1.1 split-GFP cells as measured by flow cytometry. GFP-intensity is normalized to siControl condition. Significance is calculated using a two-tailed t-test with Welsh correction; p = 0.0002.

(D) Western blots of inducible HAP1 split-GFP cell lysates. After 16 h of Dox treatment, macroH2A1.2-Flag-GFP11-T2A-mCherry is expressed. The GFP-antibody recognizes the N-GFP1-10-H4 construct.

(E) Flow cytometry histograms of GFP and mCherry fluorescent intensity of HAP1 split-GFP cells with or without treatment with 1 μg/mL DOX for 16 h.

(F) Graphical representation of the haploid genetic screen. HAP1 split-GFP cells were mutagenized with gene-trap virus. The macroH2A1.2-C-GFP11 was induced by overnight addition of DOX, after which cells were fixed. The cells with the lowest and highest 5% GFP-intensities were sorted from the haploid and mCherry positive population. To identify gene-trap integration sites the genomic DNA was isolated, and integration sites were amplified and sequenced. Created with BioRender.com.

(G) Genes identified in the split-GFP haploid genetic screen. Significantly enriched genes are highlighted in dark gray, non-significant genes are marked in light gray, the positive control ATRX in dark red, members of the PRC2 complex in teal, and ANP32B in orange. The total number of unique gene-trap insertions within a gene (x-axis) is plotted against the ratio of how often insertions in a gene are found within the high GFP over the low GFP population (y-axis).

(H) Relative GFP intensity in mock and UNC1999-treated macroH2A1.2 split-GFP T-Rex cells as measured by flow cytometry. GFP-intensity is normalized to mock-treated condition. Two-tailed t-test with Welsh correction; p = 0.0315.

(I) MacroH2A1.2-H2B-binding proteins identified by mass spectrometry. Volcano plot of the difference in iBAQ intensities between empty Ni-NTA and macroH2A1.2-H2B-bound Ni-NTA pull downs in HeLa extracts. The proteins that were significantly changed in the genetic screen are highlighted in orange.

Bar graphs show average ± SEM of four independent experiments. See also Figure S1.

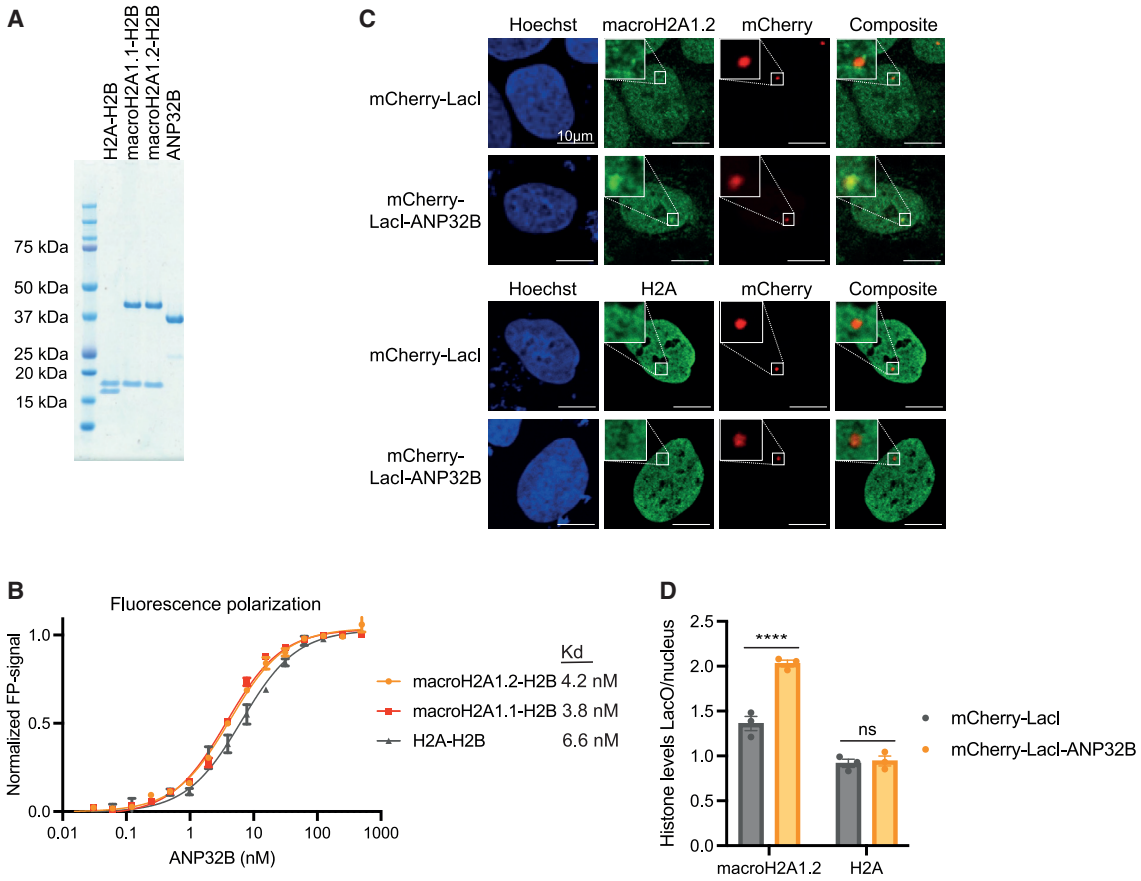

Figure 2. The histone chaperone ANP32B interacts with macroH2A

(A) Coomassie stained SDS-PAGE gel of recombinant purified ANP32B and refolded histone dimers.

(B) Fluorescence polarization assay showing binding of ANP32B to different histone dimers. The average and standard error of a total of three repeats are shown. Data were normalized 0 (no binding) to 1 (maximum binding). Binding affinities of ANP32B were calculated from raw data. Significance was calculated with a one-way ANOVA; H2A-H2B vs. macroH2A1.1-H2B $p = 0.0139$ and H2A-H2B vs. macroH2A1.2-H2B $p = 0.0302$.

(C) Representative fluorescent images of LacI experiments. U2OS LacO cells were transfected with either mCherry-LacI or mCherry-LacI-ANP32B and stained for macroH2A1.2 or H2A and Hoechst.

(D) Quantification of LacI experiments for macroH2A1.2 and H2A. The ratio of the fluorescent intensity of the histone at the LacO, as defined by the mCherry signal, over the intensity in the nucleus is plotted on the y-axis. Bar graphs show average ± SEM of 3 independent experiments each with at least 10 cells analyzed per condition. Significance is calculated using two-way ANOVA with Šidák correction; macroH2A1.2 $p < 0.0001$, H2A $p = 0.9387$.

See also Figure S2.

macroH2A dynamics on chromatin. To confirm this hypothesis, we performed Flag-HA-macroH2A1.2 immunoprecipitations in human cell extracts followed by mass spectrometry, which confirmed that ANP32B was one of the pulled down proteins with the highest normalized intensity (Figure S1H; Table S2). Moreover, ANP32B-Flag pull downs also co-immunoprecipitated endogenous macroH2A1.2 (Figure S1I). Thus, our genomics and proteomics assays suggest that ANP32B may be a histone chaperone for macroH2A.

The histone chaperone ANP32B interacts with macroH2A

To investigate the interaction between ANP32B and macroH2A, we moved to biochemical studies using recombinant human proteins (Figure 2A). Using fluorescence polarization, we first validated that our purified ANP32B binds H3-H4 with strong affinity, like previously reported (Figure S2A).[25] Interestingly, ANP32B also binds to full-length macroH2A-H2B and H2A-H2B dimers, with an affinity in the low nanomolar range (K_D = 3.8 and 6.6 nM, respectively) (Figure 2B). A 1.7-fold preference for macroH2A dimers over H2A dimers has been consistently detected. To test dimer binding preference in human cells, we characterized the effect of ANP32B toward macroH2A or H2A using the LacO/LacI system. By transfecting either mCherry-LacI or mCherry-LacI-ANP32B in LacO-containing U2OS cells, we found that all macroH2A isoforms were enriched at ANP32B-bound operons, while canonical H2A was not affected (Figures 2C, 2D, S2B, and S2C). These data indicate that ANP32B affects macroH2A localization in the nucleus. Overall, our data show that ANP32B can directly bind canonical or macroH2A-H2B dimers with high affinity *in vitro* and recruits macroH2A in cells.

ANP32B deposits macroH2A-H2B dimers

To test the function of ANP32B toward macroH2A, we postulated that ANP32B may deposit macroH2A-H2B dimers on DNA. First, we analyzed the ability of ANP32B to deposit macroH2A using the histone assembly and exchange in permeabilized cell assays.[29] We incubated permeabilized cells with recombinant ANP32B and macroH2A1.2-HA-H2B dimers, followed by immunofluorescence staining. We observed a small increase in macroH2A1.2 levels on the chromatin upon incubation with only dimers (Figures 3A and 3B), likely because of the high affinity of histone dimers for DNA. However, this signal was greatly stimulated by addition of ANP32B (Figures 3A and 3B), indicating that ANP32B can promote the deposition of macroH2A-H2B dimers in the chromatin of these pre-extracted cells.

Next, we analyzed ANP32B ability to deposit histones in a nucleosome assembly and quantification (NAQ) assay using recombinant proteins.[30] In the NAQ assay, histone chaperones are mixed with histone H3-H4 and/or H2A-H2B prior to addition of 207-bp DNA fragments containing the 601 nucleosome-positioning sequence. Nucleosome assembly depends first on tetrasome formation (i.e., deposition of $(H3\text{-}H4)_2$ tetramers on DNA), followed by H2A-H2B dimers incorporation. Indeed, nucleosomes formed efficiently in the presence of a *bona fide* tetrasome assembly factor (i.e., CAF-1), as H2A-H2B dimers can spontaneously associate with tetrasomes in these conditions[31] (Figures S3A–S3C). Strikingly, ANP32B alone does not promote tetrasome formation (i.e., deposits H3-H4 on DNA) (Figures S3B and S3C), even though it can bind to H3-H4[25] (Figures S2A). These data indicate that ANP32B cannot deposit functional $(H3\text{-}H4)_2$ tetramers on DNA. However, when combined with CAF-1, a histone H3-H4 chaperone complex, ANP32B stimulated macroH2A1.1-H2B as well as macroH2A1.2-H2B deposition onto tetrasomes (Figures 3C–3E [lane 7] and S3D–S3G). In contrast, no effect was seen on canonical H2A-H2B nucleosome formation (Figures 3C–3E [lane 6] and S3E). This implicates ANP32B in macroH2A-H2B incorporation in nucleosomes. Together, these results indicate that, even though ANP32B can bind to H3-H4 and H2A-H2B as well as macroH2A-H2B *in vitro*, this chaperone selectively contributes to the deposition of macroH2A-H2B during nucleosome assembly.

ANP32B affects macroH2A deposition in cells

Finally, we wanted to test whether ANP32B is involved in the deposition of macroH2A in human cells. Indeed, RNAi-mediated ANP32B knockdown experiments in the split-GFP T-Rex cells showed that ANP32B greatly affected the deposition of macroH2A1.1 and macroH2A1.2, to the same extent as Hells (Figure 1C), but only mildly affected canonical H2A (Figures 4A and S4A). Furthermore, mono- and di-nucleosomes extracted from MNase-digested ANP32B-depleted split-GFP cells showed a robust reduction in GFP intensity compared with the siControl condition (Figures 4B, S4B, and S4C).

To further test the effect of ANP32B on macroH2A distribution into chromatin, we performed chromatin immunoprecipitation (ChIP)-qPCR assays and found that ANP32B depletion decreased macroH2A1.2 levels at the analyzed genomic sites, which were both reported to be enriched for macroH2A1[32] (Figure 4C). To look at the effect of ANP32B depletion on macroH2A1 occupancy in chromatin on a genome-wide scale, we performed CUT&RUN experiments[33] in HepG2 cells using a macroH2A1 antibody.[13,32] We determined that macroH2A1 enriched regions in HepG2 control cells using epic2,[34] which is especially suited for the identification of broad domains such as those occupied by macroH2A histones.[19] In cells with reduced ANP32B, the total number of identified macroH2A1 domains was decreased while most of the macroH2A1 domains were shared between the two conditions (Figure S4D). Since no major redistribution to other genomic locations was observed, we used the macroH2A1 domains in control cells as a reference and found that ANP32B depletion leads to a decreased macroH2A1 signal (Figures 4D and S4E). Indeed, we observed many regions of decreased signal in the siANP32B condition compared with the siControl (Figure S4F, left), but a minority of loci showed an increase (Figure S4F, right). To analyze the differential macroH2A1 enrichment on chromatin in a statistical manner, we used the R package csaw,[35] which implements a read-counting strategy based on a sliding window across the genomic sequence. By comparing the siANP32B cells versus siControl, we identified 171 regions with decreased levels of macroH2A1, 1,687 that were unchanged, and 2,613 regions where the signal was indeed decreased (Figures 4E, S4G and S4H). Together, these data show that ANP32B interference generally reduces macroH2A1 presence in chromatin at many, but not all, genomic locations, making it a critical regulator of macroH2A histones in human cells.

DISCUSSION

Seeking to identify factors regulating the deposition of the large H2A variant macroH2A onto chromatin, we developed a method to detect histone deposition in cells in a high-throughput manner and identified and confirmed ANP32B as a macroH2A histone chaperone.

Previous studies investigated the histone binding of ANP32B and found that it interacts with canonical histones.[25] However, no investigation to date has addressed potential biological and biochemical roles for ANP32B interaction with histone variants and their incorporation. We observed that, even though ANP32B has the ability to bind H3-H4 and H2A-H2B as well as macroH2A-H2B *in vitro* (Figures 2B and S2A), it specifically stimulates the deposition of macroH2A-H2B dimers (Figures 3E and S3C). An interesting question for the future is how ANP32B histone chaperone activity can be specific for certain histone variants that only differ slightly from their canonical counterparts.

In cells, the histone chaperone activity of ANP32B remains largely unstudied. Intriguingly, an initial report showed that it negatively affects transcription of the KLF5-regulated PDGF-A (platelet-derived growth factor subunit A) gene promoter.[26] As macroH2A is also associated with transcription inhibition, it is tempting to speculate that ANP32B exerts this function by depositing the atypical histone macroH2A. It will be interesting to see how the effect of ANP32B on the dynamics and turnover of chromatin-bound macroH2A affects gene transcription and cellular functioning. As the ATP-dependent chromatin remodelers Hells and ATRX and the histone chaperone complex FACT also affect macroH2A dynamics,[19–22] investigating the activity and potential interplay between these proteins on a chromatin-wide scale will help to further elucidate the mechanisms of macroH2A deposition onto chromatin and its remodeling.

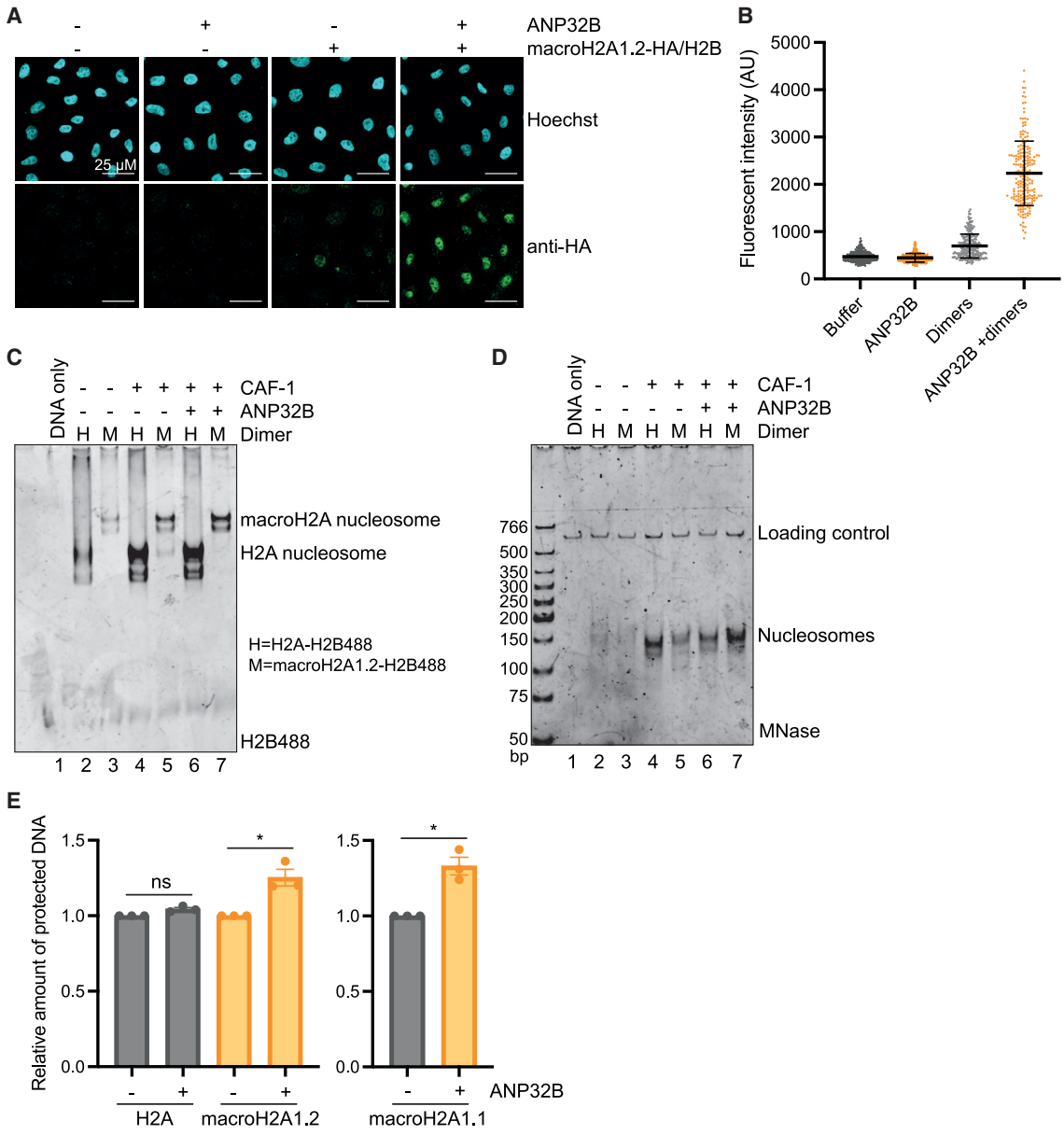

Figure 3. ANP32B has *in vitro* macroH2A histone chaperone activity

(A) Representative images of histone exchange assay. Cells were permeabilized to remove soluble proteins and incubated with or without recombinant macroH2A1.2-HA-H2B dimers and/or ANP32B. MacroH2A1.2-HA-H2B incorporation was visualized by HA staining.

(B) Quantification of histone exchange assay testing ANP32B activity toward macroH2A-H2B dimers. More than 200 cells were imaged for each condition, of which the average fluorescent intensity with standard deviation are plotted. A representative experiment out of the four repeats is shown.

(C) Native gel of representative NAQ assay showing H2B-488 signals. H3-H4 tetramers are first added to naked DNA with CAF-1ΔKER, after which H2A-H2B (H) or macroH2A-H2B (M) dimers were added with or without ANP32B.

(D) Native gel stained with SYBR Gold to visualize the MNase-protected DNA fragments of nucleosomes assembled in the NAQ assay showed in (C). Before DNA purification, a loading control of 621 bp was added to the samples.

(E) Quantification of MNase digestion-protected DNA representing the amount of H2A-H2B, macroH2A1.2-H2B or macroH2A1.1-H2B nucleosomes formed in presence or absence of ANP32B. The amount of DNA is measured with a bioanalyzer and normalized to the loading control DNA. Fragments with sizes between 125 and 160 bp are included in the quantification. Average of three independent experiments, normalized to the no ANP32B conditions, with SEM is shown. A two-tailed t-test with Welsh correction is used to calculate significance; H2A-H2B p = 0.0587, macroH2A1.2-H2B p = 0.0437, macroH2A1.1-H2B p = 0.0301. See also Figure S3.

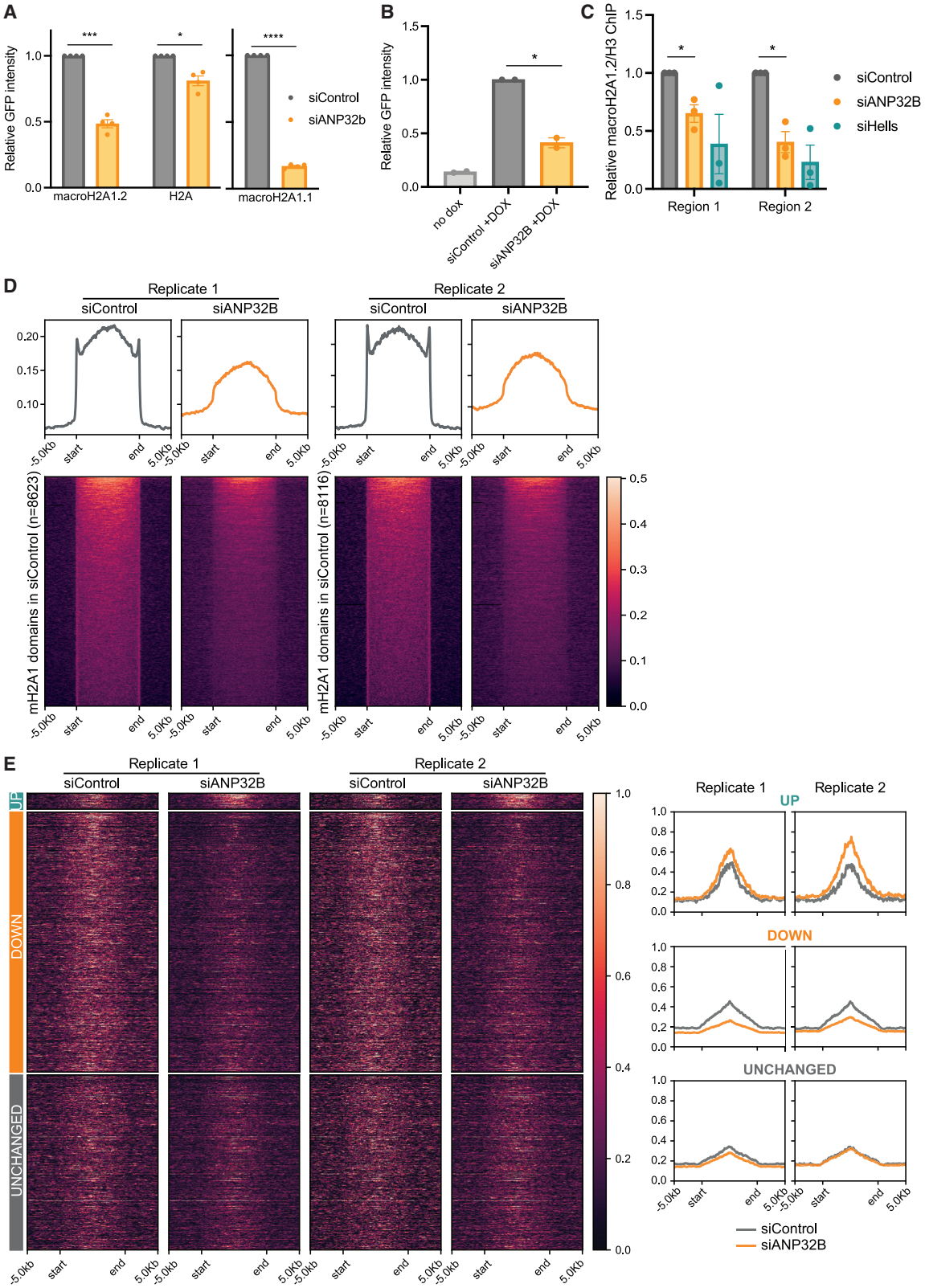

(legend on next page)

Limitations of the study

When using the split-GFP system to measure histone deposition, it is important to control for the expression of both split-GFP constructs. In our screen, we only ensured expression of the doxycycline-inducible construct, while the expression levels of N-GFP-H4 was not directly controlled. This may have led to false-positive and -negative hits in our screen, which inversely affected N-GFP-H4 levels instead of impacting macroH2A deposition. Thus, this should be checked independently for all hits of our screen, as we did for ANP32B. Similarly, the link we uncovered between PRC2 and macroH2A deposition needs to be investigated further. How ANP32B is specific for macroH2A is still not completely clear. In our histone deposition assays, we observed that, out of all the histone pairs tested, ANP32B only deposited macroH2A, yet was able to bind all different histone proteins *in vitro*. Future research will be able to dissect how histone interaction (binding) and histone deposition (function) are regulated, which domains of ANP32B are involved in this process, and whether the incorporation of any other histone variants is regulated by ANP32B in cells. These are exciting future avenues to be explored.

STAR★METHODS

Detailed methods are provided in the online version of this paper and include the following:

SUPPLEMENTAL INFORMATION

Supplemental information can be found online at https://doi.org/10.1016/j.celrep.2023.113300.

ACKNOWLEDGMENTS

We would like to thank Carla Margulies, all members of the Ladurner and Mattiroli labs, and the Department of Physiological Chemistry for productive discussions. Thanks to Jan Dreyer, Inge Rondeel, and Rosanne van Hooijdonk for assistance with experiments. We thank the Bioimaging, Biophysics, and Flow Cytometry Core Facilities of the LMU Biomedical Center for training and use of their resources. We acknowledge the Protein Analytics Unit at the Biomedical Center, Ludwig-Maximilians University Munich (DFG, RI-00089), for providing services and assistance with data analysis. We thank the Histone Source at Colorado State University for the purification of human histones. pCAGGS-ANP32B was a kind gift from Wendy Barclay and pET29a-YS14 was a kind gift from Jung-Hyun Min (Addgene plasmid # 66890). pQCXIP-GFP1-10 was a gift from Yutaka Hata (Addgene plasmid # 68715) and pRK-flag-GFP11 from Yihong Ye (Addgene plasmid # 78590). This work was supported by funding from the Dutch Research Council (VI.Veni.212.052 to I.K.M.), the European Commission (ERC StG 851564 to F.M.; ERC StG 804182 to L.T.J.), the DFG (German Research Foundation) through Project-ID 213249687 - SFB 1064 and Project-ID 325871075 - SFB 1309, as well as LMU (to A.G.L.) and the national grant PID2021-126907NB-I00 from FEDER/Ministerio de Ciencia e Innovación (MCIN) - Agencia Estatal de Investigación and the Fundació La Marató de TV3 257/C/2019 (to M.B.).

AUTHOR CONTRIBUTIONS

Conceptualization: I.K.M. and A.G.L.; methodology: I.K.M., C.R. F.M., E.F., and L.T.J.; investigation: I.K.M., E.F., D.C., and C.K.; resources: C.R.; writing - original draft: I.K.M.; writing - review and editing: F.M. and A.G.L.; supervision: L.T.J., F.M., M.B., and A.G.L.; funding acquisition: I.K.M., L.T.J., M.B., F.M., and A.G.L.

DECLARATION OF INTERESTS

A.G.L. is a founder, CSO, and managing director of Eisbach Bio GmbH, a biotechnology company in oncology and virology.

Figure 4. ANP32B affects macroH2A deposition in cells

(A) Relative split-GFP intensity of T-Rex split-GFP cells after siControl or siANP32B treatment. Average and SEM of four independent experiments are shown. Significance is calculated using two-tailed t-tests with Welsh correction; macroH2A1.1 $p < 0.0001$, macroH2A1.2 $p = 0.0005$, H2A $p = 0.0142$.

(B) Quantification of GFP signal from nucleosomes from MNase-digested split-GFP cells. Average and standard deviation of two independent experiments is shown. Two-tailed t-tests with Welsh correction $p = 0.05$.

(C) MacroH2A1.2 chromatin immunoprecipitation (ChIP)-qPCR data from HepG2 cells after siControl, siANP32B, or siHells treatment. Data were normalized to H3 ChIP and siControl conditions. Mean and error of three independent experiments are shown. Significance is calculated using two-tailed t-tests with Welsh correction siControl vs. siANP32B $p = 0.0438$.

(D) Heatmap and mean profile visualization of the mH2A1 CUT&RUN signal on the epic2 enriched domains. Domain calling was performed in the siControl sample separately for each experimental replicate. Each region is scaled to the same size and extended ±5 kb on each side.

(E) Heatmap and mean profile visualization of the mH2A1 CUT&RUN signals at the differentially bound regions identified in Figure S4H in each sample for both experimental replicates. See also Figure S4.

INCLUSION AND DIVERSITY

We support inclusive, diverse, and equitable conduct of research.

Received: February 3, 2023
Revised: August 25, 2023
Accepted: October 3, 2023
Published: October 19, 2023

REFERENCES

1. Luger, K., Mäder, A.W., Richmond, R.K., Sargent, D.F., and Richmond, T.J. (1997). Crystal structure of the nucleosome core particle at 2.8 Å resolution. Nature *389*, 251–260. https://doi.org/10.1038/38444.
2. Martire, S., and Banaszynski, L.A. (2020). The roles of histone variants in fine-tuning chromatin organization and function. Nat. Rev. Mol. Cell Biol. *21*, 522–541. https://doi.org/10.1038/s41580-020-0262-8.
3. Karras, G.I., Kustatscher, G., Buhecha, H.R., Allen, M.D., Pugieux, C., Sait, F., Bycroft, M., and Ladurner, A.G. (2005). The macro domain is an ADP-ribose binding module. EMBO J. *24*, 1911–1920. https://doi.org/10.1038/sj.emboj.7600664.
4. Kustatscher, G., Hothorn, M., Pugieux, C., Scheffzek, K., and Ladurner, A.G. (2005). Splicing regulates NAD metabolite binding to histone macroH2A. Nat. Struct. Mol. Biol. *12*, 624–625. https://doi.org/10.1038/nsmb956.
5. Ruiz, P.D., Hamilton, G.A., Park, J.W., and Gamble, M.J. (2019). MacroH2A1 regulation of Poly(ADP-Ribose) synthesis and stability prevents necrosis and promotes DNA repair. Mol. Cell Biol. *40*, e00230-19. https://doi.org/10.1128/MCB.00230-19.
6. Sebastian, R., Hosogane, E.K., Sun, E.G., Tran, A.D., Reinhold, W.C., Burkett, S., Sturgill, D.M., Gudla, P.R., Pommier, Y., Aladjem, M.I., and Oberdoerffer, P. (2020). Epigenetic regulation of DNA repair pathway choice by MacroH2A1 splice variants ensures genome stability. Mol. Cell *79*, 836–845.e7. https://doi.org/10.1016/j.molcel.2020.06.028.
7. Chen, H., Ruiz, P.D., Novikov, L., Casill, A.D., Park, J.W., and Gamble, M.J. (2014). MacroH2A1.1 and PARP-1 cooperate to regulate transcription by promoting CBP-mediated H2B acetylation. Nat. Struct. Mol. Biol. *21*, 981–989. https://doi.org/10.1038/nsmb.2903.
8. Chakravarthy, S., Gundimella, S.K.Y., Caron, C., Perche, P.Y., Pehrson, J.R., Khochbin, S., and Luger, K. (2005). Structural characterization of the histone variant macroH2A. Mol. Cell Biol. *25*, 7616–7624. https://doi.org/10.1128/MCB.25.17.7616-7624.2005.
9. Chakravarthy, S., and Luger, K. (2006). The histone variant macro-H2A preferentially forms "hybrid nucleosomes. J. Biol. Chem. *281*, 25522–25531. https://doi.org/10.1074/jbc.M602258200.
10. Kozlowski, M., Corujo, D., Hothorn, M., Guberovic, I., Mandemaker, I.K., Blessing, C., Sporn, J., Gutierrez-Triana, A., Smith, R., Portmann, T., et al. (2018). MacroH2A histone variants limit chromatin plasticity through two distinct mechanisms. EMBO Rep. *19*, e44445. https://doi.org/10.15252/embr.201744445.
11. Doyen, C.M., An, W., Angelov, D., Bondarenko, V., Mietton, F., Studitsky, V.M., Hamiche, A., Roeder, R.G., Bouvet, P., and Dimitrov, S. (2006). Mechanism of Polymerase II transcription repression by the histone variant macroH2A. Mol. Cell Biol. *26*, 1156–1164. https://doi.org/10.1128/MCB.26.3.1156-1164.2006.
12. Cong, R., Das, S., Douet, J., Wong, J., Buschbeck, M., Mongelard, F., and Bouvet, P. (2014). macroH2A1 histone variant represses rDNA transcription. Nucleic Acids Res. *42*, 181–192. https://doi.org/10.1093/nar/gkt863.
13. Buschbeck, M., Uribesalgo, I., Wibowo, I., Rué, P., Martin, D., Gutierrez, A., Morey, L., Guigó, R., López-Schier, H., and Di Croce, L. (2009). The histone variant macroH2A is an epigenetic regulator of key developmental genes. Nat. Struct. Mol. Biol. *16*, 1074–1079. https://doi.org/10.1038/nsmb.1665.
14. Gamble, M.J., Frizzell, K.M., Yang, C., Krishnakumar, R., and Kraus, W.L. (2010). The histone variant macroH2A1 marks repressed autosomal chromatin, but protects a subset of its target genes from silencing. Genes Dev. *24*, 21–32. https://doi.org/10.1101/gad.1876110.
15. Costanzi, C., and Pehrson, J.R. (1998). Histone macroH2A1 is concentrated in the inactive X chromosome of female mammals. Nature *393*, 599–601. https://doi.org/10.1038/31275.
16. Chadwick, B.P., and Willard, H.F. (2001). Histone H2A variants and the inactive X chromosome: identification of a second macroH2A variant. Hum. Mol. Genet. *10*, 1101–1113. https://doi.org/10.1093/hmg/10.10.1101.
17. Costanzi, C., and Pehrson, J.R. (2001). MACROH2A2, a new member of the MACROH2A core histone family. J. Biol. Chem. *276*, 21776–21784. https://doi.org/10.1074/jbc.M010919200.
18. Gaspar-Maia, A., Qadeer, Z.A., Hasson, D., Ratnakumar, K., Leu, N.A., Leroy, G., Liu, S., Costanzi, C., Valle-Garcia, D., Schaniel, C., et al. (2013). MacroH2A histone variants act as a barrier upon reprogramming towards pluripotency. Nat. Commun. *4*, 1565. https://doi.org/10.1038/ncomms2582.
19. Sun, Z., Filipescu, D., Andrade, J., Gaspar-Maia, A., Ueberheide, B., and Bernstein, E. (2018). Transcription-associated histone pruning demarcates macroH2A chromatin domains. Nat. Struct. Mol. Biol. *25*, 958–970. https://doi.org/10.1038/s41594-018-0134-5.
20. Ratnakumar, K., Duarte, L.F., LeRoy, G., Hasson, D., Smeets, D., Vardabasso, C., Bönisch, C., Zeng, T., Xiang, B., Zhang, D.Y., et al. (2012). ATRX-mediated chromatin association of histone variant macroH2A1 regulates alpha-globin expression. Genes Dev. *26*, 433–438. https://doi.org/10.1101/gad.179416.111.
21. Ni, K., Ren, J., Xu, X., He, Y., Finney, R., Braun, S.M.G., Hathaway, N.A., Crabtree, G.R., and Muegge, K. (2020). LSH mediates gene repression through macroH2A deposition. Nat. Commun. *11*, 5647. https://doi.org/10.1038/s41467-020-19159-0.
22. Ni, K., and Muegge, K. (2021). LSH catalyzes ATP-driven exchange of histone variants macroH2A1 and macroH2A2. Nucleic Acids Res. *49*, 8024–8036. https://doi.org/10.1093/nar/gkab588.
23. Staller, E., Sheppard, C.M., Neasham, P.J., Mistry, B., Peacock, T.P., Goldhill, D.H., Long, J.S., and Barclay, W.S. (2019). ANP32 proteins are essential for influenza virus replication in human cells. J. Virol. *93*, e00217-19. https://doi.org/10.1128/JVI.00217-19.
24. Obri, A., Ouararhni, K., Papin, C., Diebold, M.L., Padmanabhan, K., Marek, M., Stoll, I., Roy, L., Reilly, P.T., Mak, T.W., et al. (2014). ANP32E is a histone chaperone that removes H2A.Z from chromatin. Nature *505*, 648–653. https://doi.org/10.1038/nature12922.
25. Tochio, N., Umehara, T., Munemasa, Y., Suzuki, T., Sato, S., Tsuda, K., Koshiba, S., Kigawa, T., Nagai, R., and Yokoyama, S. (2010). Solution structure of histone chaperone ANP32B: interaction with core histones H3-H4 through its acidic concave domain. J. Mol. Biol. *401*, 97–114. https://doi.org/10.1016/j.jmb.2010.06.005.
26. Munemasa, Y., Suzuki, T., Aizawa, K., Miyamoto, S., Imai, Y., Matsumura, T., Horikoshi, M., and Nagai, R. (2008). Promoter region-specific histone incorporation by the novel histone chaperone ANP32B and DNA-binding factor KLF5. Mol. Cell Biol. *28*, 1171–1181. https://doi.org/10.1128/MCB.01396-07.
27. Kamiyama, D., Sekine, S., Barsi-Rhyne, B., Hu, J., Chen, B., Gilbert, L.A., Ishikawa, H., Leonetti, M.D., Marshall, W.F., Weissman, J.S., and Huang, B. (2016). Versatile protein tagging in cells with split fluorescent protein. Nat. Commun. *7*, 11046. https://doi.org/10.1038/ncomms11046.
28. Kim, J., Shin, Y., Lee, S., Kim, M., Punj, V., Lu, J.F., Shin, H., Kim, K., Ulmer, T.S., Koh, J., et al. (2018). Regulation of Breast Cancer-Induced Osteoclastogenesis by MacroH2A1.2 Involving EZH2-Mediated H3K27me3. Cell Rep. *24*, 224–237. https://doi.org/10.1016/j.celrep.2018.06.020.
29. Kimura, H., Takizawa, N., Allemand, E., Hori, T., Iborra, F.J., Nozaki, N., Muraki, M., Hagiwara, M., Krainer, A.R., Fukagawa, T., and Okawa, K. (2006). A novel histone exchange factor, protein phosphatase 2Cgamma, mediates the exchange and dephosphorylation of H2A-H2B. J. Cell Biol. *175*, 389–400. https://doi.org/10.1083/jcb.200608001.

30. Mattiroli, F., Gu, Y., and Luger, K. (2018). Measuring nucleosome assembly activity in vitro with the nucleosome assembly and quantification (NAQ) assay. Bio. Protoc. *8*, e2714. https://doi.org/10.21769/BioProtoc.2714.

31. Mattiroli, F., Gu, Y., Yadav, T., Balsbaugh, J.L., Harris, M.R., Findlay, E.S., Liu, Y., Radebaugh, C.A., Stargell, L.A., Ahn, N.G., et al. (2017). DNA-mediated association of two histone-bound complexes of yeast Chromatin Assembly Factor-1 (CAF-1) drives tetrasome assembly in the wake of DNA replication. Elife *6*, e22799. https://doi.org/10.7554/eLife.22799.

32. Douet, J., Corujo, D., Malinverni, R., Renauld, J., Sansoni, V., Posavec Marjanović, M., Cantariño, N., Valero, V., Mongelard, F., Bouvet, P., et al. (2017). MacroH2A histone variants maintain nuclear organization and heterochromatin architecture. J. Cell Sci. *130*, 1570–1582. https://doi.org/10.1242/jcs.199216.

33. Skene, P.J., and Henikoff, S. (2017). An efficient targeted nuclease strategy for high-resolution mapping of DNA binding sites. Elife *6*, e21856. https://doi.org/10.7554/eLife.21856.

34. Stovner, E.B., and Sætrom, P. (2019). epic2 efficiently finds diffuse domains in ChIP-seq data. Bioinformatics *35*, 4392–4393. https://doi.org/10.1093/bioinformatics/btz232.

35. Lun, A.T.L., and Smyth, G.K. (2016). csaw: a Bioconductor package for differential binding analysis of ChIP-seq data using sliding windows. Nucleic Acids Res. *44*, e45. https://doi.org/10.1093/nar/gkv1191.

36. Sporn, J.C., Kustatscher, G., Hothorn, T., Collado, M., Serrano, M., Muley, T., Schnabel, P., and Ladurner, A.G. (2009). Histone macroH2A isoforms predict the risk of lung cancer recurrence. Oncogene *28*, 3423–3428. https://doi.org/10.1038/onc.2009.26.

37. Cox, J., and Mann, M. (2008). MaxQuant enables high peptide identification rates, individualized p.p.b.-range mass accuracies and proteome-wide protein quantification. Nat. Biotechnol. *26*, 1367–1372. https://doi.org/10.1038/nbt.1511.

38. Schindelin, J., Arganda-Carreras, I., Frise, E., Kaynig, V., Longair, M., Pietzsch, T., Preibisch, S., Rueden, C., Saalfeld, S., Schmid, B., et al. (2012). Fiji: an open-source platform for biological-image analysis. Nat. Methods *9*, 676–682. https://doi.org/10.1038/nmeth.2019.

39. Langmead, B., Trapnell, C., Pop, M., and Salzberg, S.L. (2009). Ultrafast and memory-efficient alignment of short DNA sequences to the human genome. Genome Biol. *10*, R25. https://doi.org/10.1186/gb-2009-10-3-r25.

40. Ramírez, F., Dündar, F., Diehl, S., Grüning, B.A., and Manke, T. (2014). deepTools: a flexible platform for exploring deep-sequencing data. Nucleic Acids Res. *42*, W187–W191. https://doi.org/10.1093/nar/gku365.

41. Shim, Y., Duan, M.R., Chen, X., Smerdon, M.J., and Min, J.H. (2012). Polycistronic coexpression and nondenaturing purification of histone octamers. Anal. Biochem. *427*, 190–192. https://doi.org/10.1016/j.ab.2012.05.006.

42. Kodaka, M., Yang, Z., Nakagawa, K., Maruyama, J., Xu, X., Sarkar, A., Ichimura, A., Nasu, Y., Ozawa, T., Iwasa, H., et al. (2015). A new cell-based assay to evaluate myogenesis in mouse myoblast C2C12 cells. Exp. Cell Res. *336*, 171–181. https://doi.org/10.1016/j.yexcr.2015.06.015.

43. Lee, J.G., Takahama, S., Zhang, G., Tomarev, S.I., and Ye, Y. (2016). Unconventional secretion of misfolded proteins promotes adaptation to proteasome dysfunction in mammalian cells. Nat. Cell Biol. *18*, 765–776. https://doi.org/10.1038/ncb3372.

44. Janicki, S.M., Tsukamoto, T., Salghetti, S.E., Tansey, W.P., Sachidanandam, R., Prasanth, K.V., Ried, T., Shav-Tal, Y., Bertrand, E., Singer, R.H., and Spector, D.L. (2004). From silencing to gene expression: real-time analysis in single cells. Cell *116*, 683–698. https://doi.org/10.1016/s0092-8674(04)00171-0.

45. Fessler, E., Eckl, E.M., Schmitt, S., Mancilla, I.A., Meyer-Bender, M.F., Hanf, M., Philippou-Massier, J., Krebs, S., Zischka, H., and Jae, L.T. (2020). A pathway coordinated by DELE1 relays mitochondrial stress to the cytosol. Nature *579*, 433–437. https://doi.org/10.1038/s41586-020-2076-4.

46. Jae, L.T., Raaben, M., Herbert, A.S., Kuehne, A.I., Wirchnianski, A.S., Soh, T.K., Stubbs, S.H., Janssen, H., Damme, M., Saftig, P., et al. (2014). Virus entry. Lassa virus entry requires a trigger-induced receptor switch. Science *344*, 1506–1510. https://doi.org/10.1126/science.1252480.

47. Fessler, E., Krumwiede, L., and Jae, L.T. (2022). DELE1 tracks perturbed protein import and processing in human mitochondria. Nat. Commun. *13*, 1853. https://doi.org/10.1038/s41467-022-29479-y.

48. Mattiroli, F., Gu, Y., Balsbaugh, J.L., Ahn, N.G., and Luger, K. (2017). The Cac2 subunit is essential for productive histone binding and nucleosome assembly in CAF-1. Sci. Rep. *7*, 46274. https://doi.org/10.1038/srep46274.

49. Rouillon, C., Eckhardt, B.V., Kollenstart, L., Gruss, F., Verkennis, A.E.E., Rondeel, I., Krijger, P.H.L., Ricci, G., Biran, A., van Laar, T., et al. (2023). CAF-1 deposits newly synthesized histones during DNA replication using distinct mechanisms on the leading and lagging strands. Nucleic Acids Res. *51*, 3770–3792. https://doi.org/10.1093/nar/gkad171.

50. Meers, M.P., Bryson, T.D., Henikoff, J.G., and Henikoff, S. (2019). Improved CUT&RUN chromatin profiling tools. Elife *8*, e46314. https://doi.org/10.7554/eLife.46314.

51. Nordin, A., Zambanini, G., Pagella, P., and Cantù, C. (2023). The CUT&RUN suspect list of problematic regions of the genome. Genome Biol. *24*, 185. https://doi.org/10.1186/s13059-023-03027-3.

52. Lun, A.T.L., and Smyth, G.K. (2015). From reads to regions: a Bioconductor workflow to detect differential binding in ChIP-seq data. F1000Res *4*, 1080. https://doi.org/10.12688/f1000research.7016.2.

53. Amemiya, H.M., Kundaje, A., and Boyle, A.P. (2019). The ENCODE Blacklist: Identification of Problematic Regions of the Genome. Sci. Rep. *9*, 9354. https://doi.org/10.1038/s41598-019-45839-z.

54. Lowary, P.T., and Widom, J. (1998). New DNA sequence rules for high affinity binding to histone octamer and sequence-directed nucleosome positioning. J. Mol. Biol. *276*, 19–42. https://doi.org/10.1006/jmbi.1997.1494.

STAR★METHODS

KEY RESOURCES TABLE

REAGENT or RESOURCE	SOURCE	IDENTIFIER
Antibodies		
Mouse monoclonal anti-Flag	Sigma-Aldrich	Cat# F1804 AB_262044; RRID:AB_262044
Mouse anti-macroH2A1.2	The Ladurner laboratory	N/A
Rabbit polyclonal anti-mCherry	Thermo Fisher Scientific	Cat# PA5-34974; RRID:AB_2552323
Rabbit polyclonal anti-GFP	Abcam	Cat# ab290; RRID:AB_303395
Mouse monoclonal anti-alpha-Tubulin	Sigma-Aldrich	Cat# T5168; RRID:AB_477579
Rabbit polyclonal anti-Hells	Proteintech	Cat# 11955-1-AP; RRID:AB_2117529
Rabbit polyclonal anti-H2A	Abcam	Cat# ab18255; RRID:AB_470265
Peroxidase-AffiniPure Goat Anti-Rabbit IgG (H + L)	Jackson ImmunoResearch Labs	Cat# 111-035-003; RRID:AB_2313567
Peroxidase-AffiniPure Rabbit Anti-Mouse IgG (H + L)	Jackson ImmunoResearch Labs	Cat# 315-035-003; RRID:AB_2340061
Mouse anti-macroH2A2	Sporn et al.[36]	N/A
Rabbit polyclonal anti-H2A	Abcam	Cat# ab15653; RRID:AB_732909
Goat anti-Mouse IgG (H + L) Cross-Adsorbed Secondary Antibody, Alexa Fluor™ 488	Thermo Fisher Scientific	Cat# A-11001; RRID:AB_2534069
Goat anti-Rabbit IgG (H + L) Cross-Adsorbed Secondary antibody, Alexa Fluor™ 488	Thermo Fisher Scientific	Cat# A-11008; RRID:AB_143165
Mouse monoclonal anti-H3	Active Motif	Cat# 61475; RRID:AB_2687473
Anti-macroH2A1	Buschbeck et al.[13]	N/A
Rabbit-IgG-control	Abcam	Cat# ab46540; RRID:AB_2614925
Mouse anti-HA	Gift from Heinrich Flaswinkel, LMU Munich	N/A
Bacterial and virus strains		
DH5α competent cells	Keep in lab	N/A
BL21 DE3 pLYS competent cells	Keep in lab	N/A
Chemicals, peptides, and recombinant proteins		
Doxycycline	Sigma/Merck	D9891-1G
UNC1999	Cayman Chemical	14621
Xtreme gene HP transfection reagent	Merck	6366244001
FuGENE HD	Promega	E2311
RNAiMax	Invitrogen	13778075
MNase	Worthington-Biochem	LS004798
MNase	NEB	M0247S
Methanol-free formaldehyde	Thermo Fisher Scientific	28908
CNBr-activated Sepharose	Cytiva	GE17-0430-01
Ni-NTA	Qiagen	30210
Anti-FLAG-M2 affinity gel	Sigma	A2220
benzonase	Sigma	E1014
Alexa Fluor 488. Maleimide	Thermo Fisher Scientific	A10254
Pierce™ Protein G Magnetic Beads	Thermo Fisher Scientific	88847
Agencourt AMPure XP beads	Beckman Coulter	A63880
PowerUP SYBR Green mastermix	Thermo Fisher Scientific	A25742
pA/G-MNase	Epicypher	15–1016
SYBR Gold	Invitrogen	S11494

(*Continued on next page*)

Continued

REAGENT or RESOURCE	SOURCE	IDENTIFIER
DMEM high glucose	Sigma	D5671
FCS	gibco	10270106
Glutamine	gibco	25030024
penicillin/streptomycin	gibco	15140122
IMDM	Thermo Fisher Scientific	12440053
Hygromycin B	Thermo Fisher Scientific	10687010
Neomycin/G418	Sigma	4727878001
Hoechst 33342	Fisher Scientific	H3570
RNase A	Thermo Fisher Scientific	EN0531
Proteinase K	NEB	P8107S
macroH2A1.2-HA-H2B dimers	This study	N/A
His-macroH2A1.2-H2B dimers	This study	N/A
ANP32B	This study	N/A
Yeast CAF-1ΔKER	This study	N/A
H2A	The Histone Source, Colorado State University	HH2A
H2B T115C	The Histone Source, Colorado State University	HH2B_T115C
H3	The Histone Source, Colorado State University	HH3
H4	The Histone Source, Colorado State University	HH4
macroH2A1.1	The Histone Source, Colorado State University	N/A
macroH2A1.2	The Histone Source, Colorado State University	MACRO_H2A_1.2
Critical commercial assays		
MinElute PCR purification kit	Qiagen	28006
QIAmp DNA mini kit	Qiagen	51306
ChIP DNA Clean & Concentrator	Zymo Research	D5205
KAPA HyperPrep kit	Roche	KK8504
NEXTflex DNA barcodes for Illumina	Bioo Scientific	514101
KAPA Library Quantification kit	Roche	KK4824
Bioanalyzer high sensitivity DNA kit	Agilent Technologies	5067–4626
Deposited data		
Raw and analyzed CUT&RUN data	This paper	GEO: GSE241387
Raw haploid genetic screen sequencing data	This paper	SRA: PRJNA1022494
Raw mass spectrometry data	This paper	ProteomeXchange: PXD045696
Experimental models: Cell lines		
Human: Hek 293T	ATCC	CRL-3216
Human: U2OS LacO	The Ladurner laboratory	N/A
Human: HAP1	The Jae laboratory	N/A
Human: T-REX 293	Thermo Fisher Scientific	R71007
Human: HepG2	DSMZ	ACC 180
Human: HeLa S3	ATCC	CCL-2.2
Oligonucleotides		
siControl: 5′-UGGUUUACAUGUCGACUAA-3	This study	N/A

(*Continued on next page*)

Continued

REAGENT or RESOURCE	SOURCE	IDENTIFIER
siANP32B: 5′UGACUACCGAGAGAGUGUCUU-3′	This study	N/A
siHells: 5′-GAAGUGAAUAUCCCUGUAGdTdT-3′	This study	N/A
qPCR location 1 fw: GCGAGCATAATCTCCTGAATC	This study	N/A
qPCR location 1 rev: CTCCCGTGTGGATGTTTACC	This study	N/A
qPCR location 2 fw: CAGGCGTGTCTTTAGGATGTAG	This study	N/A
qPCR location 2 rev: TGCCACTGACGTGATGATATG	This study	N/A
Recombinant DNA		
pmCherry-C1-LacI-ANP32B	This study	N/A
pEMT11-His-ANP32B	This study	N/A
pET29a-macroH2A1.2-HA-H2B	This study	N/A
pRK-GFP1-10-H4	This study	N/A
pLenti6-GFP1-10-H4	This study	N/A
pLIX-macroH2A1.2-GFP11-T2A-mCherry	This study	N/A
pcDNA5/FRT/TO-H2A-Flag-GFP11	This study	N/A
pcDNA5/FRT/TO-macroH2A1.1-Flag-GFP11	This study	N/A
pcDNA5/FRT/TO-macroH2A1.2-Flag-GFP11	This study	N/A
pCAGGS-ANP32B	Gift from Wendy Barclay	N/A
Software and algorithms		
FlowJo	BD Biosciences	https://www.flowjo.com/
MaxQuant 2.1.0.0	Cox & Mann[37]	https://www.maxquant.org/
Fiji	Schindelin et al.[38]	https://fiji.sc/
Bowtie2	Langmead et al.[39]	https://bowtie-bio.sourceforge.net/bowtie2/index.shtml
DeepTools	Ramirez et al.[40]	https://deeptools.readthedocs.io/en/latest/
Epic2	Stovner & Saetrom[34]	https://github.com/biocore-ntnu/epic2
Csaw	Lun & Smyth[35]	https://bioconductor.org/packages/release/bioc/html/csaw.html
Other		
Black walled 384 well plate	Corning	CLS3575-50EA
HisTrap HP column	Cytiva	17524701
HiLoad 16/600 superdex200 pg	Cytiva	28989335
HiTrap Q HP column	GE Healthcare	17-1154-01

RESOURCE AVAILABILITY

Lead contact

Further information and requests for resources and reagents should be directed to and will be fulfilled by the lead contact, Andreas Ladurner (andreas.ladurner@bmc.med.lmu.de).

Materials availability

Plasmids generated in this study are available from the lead contact upon request.

Data and code availability

- Raw and processed CUT&RUN data is available in the Gene Expression Omnibus, GEO: GSE241387.

- Raw haploid genetic screen data is available in the Sequence Read Archive, SRA: PRJNA1022494
- Raw mass spectrometry data is deposited to the ProteomeXchange Consortium via the PRIDE partner repository. ProteomeXchange: PXD045696
- This paper does not report any original code.
- Any additional information required to reanalyze the data reported in this work paper is available from the lead contact upon request.

EXPERIMENTAL MODEL AND STUDY PARTICIPANT DETAILS

The following human cell lines have been used in this study: Hek 293T (F), U2OS LacO (F), HAP1 (M), T-REX 293 (F), HepG2 (M) and HeLa S3 (F). HAP1 cells were cultured in IMDM (Thermo Fisher Scientific) supplemented with 10% heat-inactivated FCS (Thermo Fisher Scientific) and 1% penicillin/streptomycin/glutamine (Thermo Fisher Scientific). All other cells were cultured in high glucose DMEM (Sigma) culture media supplemented with 10% Fetal Calf Serum (FCS, GIBCO), 2 mM glutamine (GIBCO) and 1% penicillin/streptomycin (GIBCO). Cells were grown in humidified incubators at 37°C and 5% CO_2 and tested bimonthly for mycoplasma infections.

METHOD DETAILS

Constructs

ANP32B plasmids: pCAGGS-ANP32B was a kind gift from Wendy Barclay.[23] ANP32B DNA was amplified from the pCAGGS plasmid with NcoI and XhoI overhangs and ligated into a digested pETM11 vector or amplified with KpnI and BamHI overhangs and ligated into the pmCherry-C1-LacI vector.

pET29a-macroH2A1.2-HA-H2B: pET29a-YS14 (Addgene plasmid # 66890[41]) was digested with NcoI and EcoRI to remove H2A and a PCR product of human macroH2A1.2 cDNA[10] with NcoI and EcoRI overhangs was ligated in. Next an HA-tag was added on the C terminus of macroH2A1.2 by PCR. The resulting plasmid was digested with EcoRI and XhoI to remove the Xenopus histones H2B, H3 and H4 and a PCR product of human H2B cDNA with MfeI and XhoI overhangs was ligated in.

Split-GFP constructs: pQCXIP-GFP1-10 was a gift from Yutaka Hata (Addgene plasmid # 68715[42]). pRK-flag-GFP11 was a gift from Yihong Ye (Addgene plasmid # 78590[43]). H2A, macroH2A1.1 and macroH2A1.2 human cDNA were ligated into HindIII digested pRK-flag-GFP11. Subsequently the histone-flag-GFP11 sequences were amplified and ligated into AflII and NotI digested pcDNA5/FRT/TO (Invitrogen). To clone pRK-GFP1-10-H4, pRK-flag-GFP11 was digested with HindIII and XbaI and PCR amplified human H4 cDNA and GFP1-10 were ligated in with a SalI overhangs in between the H4 and GFP1-10. For pLIX-macroH2A1.2-GFP11, macroH2A1.2-GFP11-T2A-mCherry encoding DNA was ordered from Eurofins and ligated into SalI-BamHI digested pLIX. GFP1-10-H4 was amplified from pRK-GFP1-10-H4 with EcoRI and XbaI overhangs and ligated into the pLenti6-PGK-Puro vector.

Cell culture and treatments

The expression of histone-Flag-GFP11 was induced by the addition of 1ug/ml Doxycycline for 16–18 h for all split-GFP experiments. For EZH2 inhibition cells were treated with 5 μM UNC1999 for 20 h.

Split-GFP T-Rex 293 cells were generated by first transfecting WT T-Rex 293 with both a pOG44 Flp-Recombinase vector (Invitrogen) as well as the pcDNA5/FRT/TO Histone-Flag-GFP11 (H2A, macroH2A1.1 or macroH2A1.2) in a 4:1 ratio using Xtreme gene HP transfection reagent (Merck). After selection with 50 μg/ml Hygromycin B, cells were transfected with pRK-GFP1-10-H4 and selected with 400 μg/ml Neomycin. Single clones were tested for expression levels and inducibility with Doxycycline.

Split-GFP HAP1 cells were generated by lentiviral induction using pLenti6.UBC GFP1-10-H4 and pLIX puro macroH2A1.2-Flag-GFP11-T2A-mCherry.

For LacI experiments, U2OS cells containing LacO repeats[44] were transfected with mCherry-LacI or mCherry-LacI-ANP32B constructs using FuGENE HD (Promega). For macroH2A1.1 analysis, GFP-macroH2A1.1 was co-transfected as the cells did not express this isoform. For immunoprecipitations Hek293 T cells were transfected with pCAGGS-ANP32B-Flag using FuGENE HD according to the manufacturer's protocol. RNAi experiments were performed with RNAiMax (Invitrogen) according to the manufacturer's protocol 3 days before cell harvesting or fixation. siControl: 5′-UGGUUUACAUGUCGACUAA-3′, siANP32B: 5′UGACUACCGAGAGA GUGUCUU-3′, siHells: 5′-GAAGUGAAUAUCCCUGUAGdTdT-3'.

Nucleosome isolation from cells

Split-GFP T-Rex 293 cells were treated with 1 μg/mL doxycyline for 20h before harvesting. Cells were harvested by trypsination, washed once with PBS and resuspended at $4*10^7$ cells/ml in Buffer 1 (10 mM HEPES pH 7.9, 1.5 mM MgCl2, 10 mM KCl, 0.5 mM DTT, cOmplete EDTA-free protease inhibitor cocktail (Roche)). After 10 min on ice, 0.1% NP-40 was added followed by another 5 min incubation on ice, vortexing for 10 s and nuclei were pelleted at 3800g for 10 min. The nuclei were washed once in MNase digestion buffer (10 mM Tris-HCl pH 7.5, 15 mM NaCl, 60 mM KCl, 1 mM CaCl2, 0.15 mM spermine, 0.5 mM spermidine, cOmplete EDTA-free protease inhibitor cocktail (Roche)). The amount of chromatin was measured at an absorbance of 260 nm

with a dilution of 4 μL of nuclei in 400 μL 2M NaCl. Nuclei were resuspended in MNase digestion buffer (60 μg in 340 μL) and digested with 2U MNase (Worthington) at 37°C for 10 min. The reaction was stopped by addition of EDTA to a final concentration of 20 mM and nuclei were pelleted at 3600g for 10 min. Nucleosomes were extracted by resuspending the pellets in nucleosome extraction buffer (20 mM Tris pH 8.0, 10 mM EDTA, 0.5 mM NaCl), followed by incubation on ice for 10 min and centrifugation at 13,200 rpm for 10 min. Nucleosomes were analyzed on native PAGE. DNA was purified with MinElute kit (Qiagen) and run on a 1% agarose gel to check for chromatin digestion.

Western blotting

Whole cell extracts were prepared by lysing cells in Leammli buffer and boiling for 3 min. DNA was sheared by 5 min sonication (Diagenode Bioruptor Pico, 30 s on, 30 s off). Samples were separated on a 4–12% Bis-Tris gradient gel (Thermo Fisher Scientific) and transferred to nitrocellulose membrane (0.2 μm, Biorad). Membranes were blocked for 1 h in 5% milk in PBS and incubated with primary antibody, diluted in PBS +0.05% Tween 20, for 2 h at room temperature (RT) or overnight at 4°C. Membranes were washed 3 times 10 min in PBS-Tween, incubated with secondary antibody for 1–2 h and again washed 3 times for 10 min with PBS-Tween. Antibodies were visualized using SuperSignal West Pico PLUS Chemiluminescent Substrate (Fisher Scientific) with a ImageQuant800 imager (Amersham).

Antibodies: Mouse-*anti*-Flag (1:5000, Sigma-Aldrich, F1804), mouse-*anti*-macroH2A1.2 (1:500, homemade), rabbit-*anti*-mCherry (1:500, Invitrogen, PA5-34974), rabbit-*anti*-GFP (1:1000, Abcam, ab290), mouse-*anti*-Tubulin (1:5000, Sigma-Aldrich, T5168), rabbit-*anti*-Hells (1:500, Proteintech, 11955-1-AP), rabbit-*anti*-H2A (1:1000, Abcam, ab18255), HRP-goat-*anti*-rabbit (1:10000, Jackson Immuno Research, 111-035-003) and HRP-rabbit-*anti*-mouse (1:10000, Jackson Immuno Research, 315-035-003).

Flow cytometry

Cells were harvested by trypsinization, washed once in PBS and fixed in 4% Paraformaldehyde (PFA) at 37°C for 15 min. Cells were washed twice in 1% FCS in PBS and measured on a BD LSRFortessa (BD Biosciences). Data was analyzed using FlowJo (BD Biosciences).

Microscopy

The split-GFP cells were grown on coverslips and fixed with 4% PFA for 15 min at RT and stained with 1ug/ml Hoechst 33342 (Fisher Scientific) in PBS+ (PBS with 0.5% BSA and 0.15% glycine) for 15 min at RT. Coverslips were mounted with Aqua-Poly/Mount (Polysciences) and imaged on a Zeiss AxioObserver Z1 confocal spinning-disk microscope equipped with a sCMOS ORCA Flash 4.0 camera (Hamamatsu) and a Plan-Apochromat 40x/0.95 Korr air objective.

For the immunofluorescence experiments, cells were grown on glass coverslips, transfected as described above and fixed in 2% PFA containing 0.1% Triton for 15 min at RT. Cells were washed 3 times short and 2 times 10 min in PBS-T (PBS with 0.1% Triton) followed by a wash in PBS+. Slides were stained with mouse-*anti*-macroH2A1.2 (1:250), mouse-*anti*-macroH2A2[36] (1:100) or rabbit-*anti*-H2A (1:1000, Abcam ab15653) diluted in PBS+ for 2 h at RT and subsequently washed with PBS-T (3x short, 2 × 10 min) and once with PBS+. Secondary antibodies (goat-*anti*-mouse-488 or goat-*anti*-rabbit-488 1:1000, Thermo Fisher Scientific A-11001 or A-11008) and Hoechst 33342 were diluted in PBS+ and staining was done at RT for 1 h, followed again by washes in PBS-T and PBS+. Coverslips were mounted using Aqua-Poly/Mount (Polysciences) and imaged on an inverted Leica SP8X WLL confocal microscope equipped with an HC PL APO 40x/1.30 Oil objective. Images were analyzed using ImageJ.[38]

Haploid genetic screen

To identify regulators of macroH2A deposition, haploid genetic screening on HAP1 cells was performed as described previously.[45] HAP1 N-GFP(1–10)-H4, macroH2A1.2-FLAG-GFP11-T2A-mCherry cells were subjected to ultra-deep genome-wide mutagenesis using a variant of the gene-trap retrovirus[46] containing BFP produced in 293T cells. The retroviral particles were concentrated by ultracentrifugation at 88,800 g at 4°C for 2h and HAP1 cells were transduced three consecutive times in the presence of protamine sulfate. Subsequently, the library of mutant cells was expanded to 24 x T175 flasks, which were treated with 1 μg/mL doxycycline the day after seeding. After 16h of doxycycline treatment, cells were harvested by trypsinization, washed with PBS, strained through a 40 μm cell strainer (Greiner, 542040) prior to fixation with methanol-free 4% formaldehyde (Thermo Fisher, 28908) for 10 min at 37°C. Fixation was stopped with PBS +1% FCS, cells were counted, resuspended to 100 million cells per mL in PBS +1% FCS and counterstained with DAPI at a final concentration of 2.5 μg/mL for the identification of haploid cells based on DNA content. After three washing steps, approximately 10^7 cells of the bottom 5% GFP-low and top 5% GFP-high cells were sorted on a BD Fusion cell sorter (BD Biosciences) using a 70 μm nozzle. A non-doxycyline induced control was used to identify positive cells and to set the gates.

Genomic DNA from these sorted populations was extracted using the QIAmp DNA Mini Kit (Qiagen, 51306) following the manufacturer's instructions (de-crosslinking was performed at 56°C overnight). Cloning of gene trap insertion sites, identification of gene-trap mutations by deep sequencing and alignment to the human genome (hg19) was performed as previously reported.[47] A two-sided Fisher's exact test was used to calculate the enrichment for mutations for each affected gene in the populations with elevated or decreased GFP fluorescence. Significant regulators were identified by dividing the fraction of unique sense insertions mapping to the query gene in the GFP-high cells by the corresponding fraction of unique sense insertions in the GFP-low cells. The Benjamini-Hochberg false discovery rate correction was used to account for multiple testing. Per gene, the resulting mutation

ratio (y axis) was plotted against the combined number of identified unique insertions in the gene in the GFP-high and GFP-low cells (x axis).

Pull down macroH2A interactors

Ni-NTA was incubated with recombinant His-macroH2A1.2-H2B dimers in binding buffer (25 mM HEPES pH 8.3, 300 mM NaCl, 1 mM $MgCl_2$, 0.5% Triton X-100, 0.5 mM EDTA, 10% glycerol, cOmplete EDTA-free protease inhibitor cocktail (Roche)) for 1 h while rotating, followed by 3 washes. CNBr-activated Sepharose (Cytiva) was washed with 1 mM HCl after which macroH2A1.2-H2B dimers were coupled to the beads in 2 M NaCl, 40% glycerol, 50 mM HEPES pH 8.0. After coupling, beads were quenched with 0.1 M Tris pH8.0, 0.5 M NaCl. For pull downs, HeLa cells were lysed in IP buffer (25 mM HEPES pH 8.3, 130 mM NaCl, 1 mM $MgCl_2$, 0.5% Triton X-100, 0.5 mM EDTA, 10% glycerol, cOmplete EDTA-free protease inhibitor cocktail (Roche)) for 10 min on ice. Lysates were centrifuged for 15 min at 16.000g and supernatant was added to the Ni or CNBr beads. Samples were incubated for 2 h at 4°C while rotating, followed by three washes in IP buffer (Ni-beads were washed in IP buffer with 20mM imidazole) and 3 washes in 50 mM Tris pH8.

HeLa cells expressing Flag-HA-macroH2A1.2 were washed in PBS, lysed in IP buffer and treated with benzonase for 1h while rotating at 4°C. Lysates were cleared by spinning for 15 min at 13.000g and supernatant was incubated with anti-FLAG-M2 affinity gel (Sigma) for 2 h at 4°C while rotating. Beads were washed 3 times in IP buffer and 3 times with 50 mM Tris pH8.

LC-MS analysis

Proteomic analysis was performed at the Protein Analysis Unit (ZfP) of the Ludwig Maximilians University of Munich, a registered research infrastructure of the Deutsche Forschungsgemeinschaft (DFG, RI-00089).

Beads were washed three times with 50 mM NH_4HCO_3 and incubated with 10 ng/μL trypsin in 1 M urea 50mM NH_4HCO_3 for 30 min, washed with 50 mM NH_4HCO_3 and the supernatant digested overnight (ON) in presence of 1mM DTT. Digested peptides were alkylated and desalted prior to LC-MS analysis.

For LC-MS/MS purposes, desalted peptides were injected in an Ultimate 3000 RSLCnano system (Thermo), separated in a 15-cm analytical column (75 μm ID with ReproSil-Pur C18-AQ 2.4 μm from Dr. Maisch) with a 50-min gradient from 4 to 40% acetonitrile in 0.1% formic acid or in a 25-cm analytical column (75 μm ID, 1.6μm C18, IonOpticks) with a 50-min gradient from 2 to 37% acetonitrile in 0.1% formic acid. The effluent from the HPLC was directly electrosprayed into a Qexactive HF (Thermo) or into a Orbitrap Exploris-480 (Thermo) operated in data dependent mode to automatically switch between full scan MS and MS/MS acquisition.

For Qexactive HF measurements parameters were as follows: survey full scan MS spectra (from m/z 375–1600) were acquired with resolution R = 60,000 at m/z 400 (AGC target of $3x10^6$). The 10 most intense peptide ions with charge states between 2 and 5 were sequentially isolated to a target value of $1x10^5$, and fragmented at 27% normalized collision energy. Typical mass spectrometric conditions were: spray voltage, 1.5 kV; no sheath and auxiliary gas flow; heated capillary temperature, 250°C; ion selection threshold, 33.000 counts.

For Orbitrap Exploris-480 measurements parameters were as follows: survey full scan MS spectra (from m/z 350–1200) were acquired with resolution R = 60,000 at m/z 400 (AGC target of $3x10^6$). The 10 most intense peptide ions with charge states between 2 and 6 were sequentially isolated to a target value of $1x10^5$, and fragmented at 30% normalized collision energy. Typical mass spectrometric conditions were: spray voltage, 1.5 kV; no sheath and auxiliary gas flow; heated capillary temperature, 275°C; ion selection threshold, 33.000 counts.

MaxQuant[37] 2.1.0.0 was used to identify proteins and quantify by iBAQ with the following parameters: Database, Uniprot_UP000005640_Hsapiens_20210521; MS tol, 10ppm; MS/MS tol, 20 ppm Da; Peptide FDR, 0.1; Protein FDR, 0.01 Min. peptide Length, 7; Variable modifications, Oxidation (M); Fixed modifications, Carbamidomethyl (C); Peptides for protein quantitation, razor and unique; Min. peptides, 1; Min. ratio count, 2. Identified proteins were considered if at least 2 peptides were identified with razor + unique peptides >1.

Protein purifications

BL21 DE3 pLYS cells were transformed with pETM11-His-ANP32B and grown until OD600 = 0.7. Expression was induced by addition of 0.4 mM IPTG for 4 h at 37°C and cells were harvested by spinning at 5000g for 10 min at 4°C. Cells were lysed in 50 mL Buffer A (20 mM sodium phosphate buffer (Na2HPO4:NAH2PO4 3:1), 300 mM NaCl, 30 mM imidazole, 1 mM DTT pH7.4, 0.2 mM PMSF) by sonication. Lysates were cleared by centrifugation at 38,500 g at 4°C for 30 min. Samples were loaded on a 1 mL HisTrap HP column (Cytiva) and eluted with a gradient with buffer B (Buffer A with 300 mM imidazole). Fractions containing the ANP32B were further purified on a HiLoad 16/600 superdex200 pg (Cytiva) in buffer C (Buffer A without imidazole).

MacroH2A1.2-HA-H2B was co-expressed from the same polycistronic plasmid and purified as dimer. BL21 DE3 pLys cells containing pET29a-macroH2A1.2-HA-H2B were grown until an OD600 of 0.4 upon which 0.4 mM IPTG was added for 18 h at 37°C. Cells were harvested by centrifugation at 4,500g for 10 min at 4°C and lysed by sonication in lysis buffer (50 mM HEPES pH 8.0, 2.0 M NaCl, 30 mM imidazole, 1 mM PMSF, 0.5 mM TCEP). Lysates were cleared by centrifugation at 38,500 g at 4°C for 30 min before loading onto a 1 mL HisTrap HP column (Cytiva). Column was washed with 10 mL lysis buffer and bound proteins were eluted with high salt buffer (50 mM HEPES pH8.0, 2 M NaCl and 300 mM imidazole). His-tag was cleaved of by thrombin digestion for 18 h at 4°C. Dimers were further purified with a HiLoad 16/600 superdex200 pg (Cytiva) in 50mM HEPES pH8 and 2M NaCl.

Yeast CAF-1ΔKER(Δ146-215) was purified as described before[48,49] with the following adaptations: After the His-Trap column, the complex was purified with a HiTrapQ column and the final elution from the Superdex 200 was performed in 20 mM HEPES pH8, 200 mM NaCl, 1 mM EDTA, 1 mM TCEP.

Histone labeling and refolding

Human H2A, H2B T115C, H3, H4, macroH2A1.1 and macroH2A1.2 protein preps were purchased from The Histone Source at Colorado State University. Lyophilized histone preps were then resuspended in unfolding buffer (6M Guanidinium HCL, 20 mM Tris pH 7.5, 0.2 mM TCEP) for 1 h at RT. For labeling, Alexa Fluor 488 maleimide (Thermo Fisher Scientific, A10254) was added to H2B-T115C in a 1:1 M ratio and incubated overnight at 4°C while rotating. Labeling was stopped by the addition of DTT to a final concentration of 10mM, followed by another 1-h incubation at 4°C. To generate dimers or tetramers, histones were mixed in an equivalent molar ratio at a total concentration of 1 mg/mL and dialyzed against refolding buffer (2 M NaCl, 10 mM Tris pH 7.5, 1 mM EDTA and 0.5 mM TCEP) for 20 h at 4°C. Dialyzed sample was run over a HiLoad S200 column (Cytiva) in refolding buffer and dimer/tetramer-containing fractions were pooled and concentrated. Labeling efficiency and concentrations were analyzed using the Nanodrop One (Thermo Scientific).

Nucleosomes were assembled by mixing 207 bp DNA with H3/H4 tetramers and macroH2A1.2-H2B dimers in RB-high (2 M NaCl, 10 mM Tris pH 7.5, 1 mM EDTA, 1 mM TCEP) followed by overnight dialysis to RB-low (0.25 M NaCl, 10 mM Tris pH 7.5, 1 mM EDTA, 1 mM TCEP) and a final 2h dialysis to 20 mM Tris pH 7.5, 1 mM EDTA, 1 mM TCEP.

Fluorescence polarization assay

Experiments were carried out in a black-walled 384 well plate (Corning) in duplicate, using 30 μL reaction volume. 15 nM of fluorescently labeled histone dimers were mixed with varying concentrations of ANP32B (0–500 nM) in FP buffer (25 mM TRIS pH 7.5, 300 mM NaCl, 5% glycerol, 1 mM EDTA, 0.01% NP-40, 0.01% CHAPS, 1 mM DTT). Fluorescence polarization was measured using the CLARIOstar^{plus} (BMG Labtech) with 200 flashes of 482-16 laser, calibrated with the no-chaperone condition set as 10% of the gain value and 35 mP. Curve fitting and binding affinity calculations (Y=Bmax*X/(Kd+X) + Background) were done in Prism (Graphpad).

Immunoprecipitations

Hek293 T cells were transfected with pCAGGS-ANP32B 2 days before harvesting. Cells were washed in PBS and lysed in IP Buffer (25 mM Tris pH7.8, 130 mM NaCl, 1 mM $MgCl_2$, 0.5% Triton X-100, 0.5 mM EDTA, 10% glycerol, cOmplete EDTA-free protease inhibitor cocktail (Roche)) for 10 min on ice. Lysates were incubated with benzonase (Merck-Millipore) for 1h and cleared by centrifugation for 15 min at 13.000g. ANP32B-Flag and interacting proteins were purified by incubating with anti-FLAG-M2 affinity gel (Sigma) for 2 h at 4°C while rotating. Beads were washed 3 times in IP buffer and bound proteins were eluted by boiling in Leammli buffer for 5 min.

ChIP-qPCR

Cells were collected by trypsinization and resuspended in 5 mL PBS, followed by addition of 1/10 volume of 11% formaldehyde solution (50 mM Hepes-KOH pH7.6, 100 mM NaCl, 1 mM EDTA, 0.5 mM EGTA, 11% formaldehyde). After 10 min incubation the formaldehyde was quenched by addition of 1/10 volume of 1.25 M glycine and incubated for another 10 min. Cells were pelleted by centrifugation for 5 min at 1500 g, washed twice with PBS and lysed for 10 min on ice in nuclei lysis buffer (1% SDS, 50 mM Tris pH8, 10 mM EDTA, cOmplete EDTA-free protease inhibitors (Roche). Chromatin was sheared by sonication for 13 min, after which the sample was cleared by centrifugation for 10 min at 16000 g. For pull downs, 10 μg chromatin was mixed with 2 μL macroH2A1.2 or H3 antibody (Active Motif Cat# 61475) in a total volume of 500 μL ChIP buffer (1.1% Triton, 0.01% SDS, 167 mM NaCl, 16.7 mM Tris pH8, 1.2 mM EDTA) and incubated overnight at 4°C while rotating. Pierce Protein G Magnetic Beads (Thermo Scientific) were added for 2h and subsequently the beads were washed 3 times in low salt wash (20 mM Tris pH8, 2 mM EDTA, 1% Triton X-100, 150 mM NaCl, followed by a wash in 500 mM NaCl and a wash in LiCl buffer (10 mM Tris pH8, 1 mM EDTA, 0.25 M LiCl, 0.5% IGEPAL, 0.5% deoxycholate sodium salt). After a final wash in TE (10 mM Tris pH8, 1 mM EDTA), samples were eluted in 75 μL elution buffer (25 mM Tris pH 7.5, 10 mM EDTA, 0.5% SDS) for 1h at 65°C. Eluates were mixed with 75 μL TE and treated with RNase A and Proteinase K. DNA was isolated using Agencourt AMPure XP beads (Beckman Coulter). For the qPCR, 6 μL DNA was mixed with 7.5 μL PowerUP SYBR Green mastermix (Thermo Scientific) and 1.5 μL primer (location 1: fw GCGAGCATAATCTCCTGAATC; rev CTCCCGTGTGGATGTTTACC, location 2: fw CAGGCGTGTCTTTAGGATGTAG; rev TGCCACTGACGTGATGATATG).

CUT&RUN

CUT&RUN reactions were performed as described in Meers et al.,[50] following the "Standard CUT&RUN" protocol. Briefly, approximately 1M cryopreserved HepG2 cells were thawed and bound to concanavalin-A paramagnetic beads (Epicypher), then split equally, resuspended in antibody binding buffer and incubated overnight with either home-made macroH2A1 antibodies[13,32] and an IgG non-targeting control (Abcam ab46540). Both antibodies were diluted 1:100 in the binding reaction. Samples were then washed and bound with pA/G-MNase (Epicypher), chromatin digestion started by addition of CaCl and stopped after 30 min with STOP buffer containing chelating agents. Samples were then incubated for 30 min at 37°C to release CUT&RUN fragments,

incubated 1 h at 50°C with proteinase K and purified using ChIP DNA Clean & Concentrator (Zymo Research). Sequencing libraries were prepared with the KAPA HyperPrep kit (Roche) and NEXTflex DNA barcodes for Illumina (Bioo Scientific), quantified with the KAPA Library Quantification kit (Roche), pooled at approximately equimolar concentration and sequenced at Novogene (UK) Co Ltd. in an Illumina NovaSeq instrument to achieve a depth of at least 10M paired-end 150 bp reads per sample.

Sequencing data processing and alignment

Paired end reads were adapter and quality trimmed with trimgalore using –stringency 3 and aligned using Bowtie2[39] to UCSC hg38 (no alternative contigs) with the following options: –very-sensitive –no-discordant –no-mixed -X 700 –dovetail. The resulting alignment bam files were filtered to retain only concordant proper pair alignments using samtools and sam flag 0x2. Coverage signal profiles in bigwig format were generated using the bamCoverage function from deepTools[40] with a Counts-Per-Million per-sample normalization using a bin of 1 bp, ignoring ChrM for normalization and excluding reads falling into described "blacklisted" regions for CUT&RUN.[51] These profiles were used for visualization using deepTools computeMatrix and plotHeatmap functions.

Epic2 domain calling

Epic2[34] was used to perform peak calling in the form of broad domain detection on the filtered aligned reads using the IgG controls as background, a bin size of 1000 bp and the following options: –guess-bampe -kd -fdr 0.0001 –gaps-allowed 5. Domains were compared between samples counting overlaps where at least 20% of either one of the regions was overlapping the other.

Differential binding analysis with csaw

Differentially bound regions were identified using the R package csaw,[35] which is based on counting reads into sliding windows across the genome. The analysis was performed following the workflow guidelines provided by the authors.[52] The filtered bam files for each sample were used as input, setting as parameters: paired-end data, a maximum fragment length of 700 bp, restricted analysis to standard chromosomes. A stringent blacklist of regions was obtained by merging the CUT&RUN blacklisted regions within 10 kb[51] and the ENCODE blacklist.[53] Reads falling into the blacklist were discarded for quantification. Sliding windows for read counting were set at 10 kb with a spacing of 1 kb. Only windows with a fold-change of at least 3 over the IgG background were kept for further analysis using the filterWindowsGlobal function. The filtered windows were normalized for compositional bias using the normFactors function. Dispersion estimates and differential binding testing was performed with edgeR as described in the package documentation, using in the model a single experimental condition with two levels (siControl, siANP32B). Individual windows were merged and corrected for multiple testing with the mergeResults function and a 1000 bp maximum gap. Only regions with a combined FDR <0.05 were considered differentially bound.

Histone exchange in permeabilized cells

Protocol was adapted from.[29] HeLa cells were grown on coverslips to 70% confluency. Cells were placed on ice and washed twice with PBF (100 mM CH_3COOK pH7.4, 30 mM KCl, 10 mM Na2HPO4, 1 mM DTT, 1 mM MgCl2, 1 mM ATP, 5% Ficoll). Cells were permeabilized in PBF containing 0.2% Triton X-100 for 7 min on ice, followed by two washes in PBF. Permeabilized cells were next incubated for 1h at 37C with 1, 2 or 4 μg and 0.5 μg macroH2A1.2-HA-H2B dimers, washed twice in PBF and twice with PBS. Finally, cells were fixed for 15 min in 4% PFA and stained with mouse-*anti*-HA (1:250, kind gift from Heinrich Flaswinkel, LMU) according to the protocol described above.

Nucleosome assembly and quantification (NAQ) assay

We adapted the original NAQ protocol[30] for the analysis of H2A-H2B dimer loading. For this we first pre-loaded H3-H4 tetramers onto the DNA containing the 601 Widom sequence.[54] To this end, 0.2 μM tetramers were mixed with 0.4 μM yeast CAF-1ΔKER or ANP32B in NAQ buffer (25 mM Tris pH7.5, 150 mM NaCl, 1 mM EDTA, 0.02% Tween 20, 0.5 mM TCEP) and incubated for 10 min at room temperature. Subsequently 0.5 μM of 207 bp DNA was added followed by another 10 min incubation at room temperature. H2A-H2B488 or macroH2A1.2-H2B488 dimers were pre-mixed with ANP32B in an equivalent molar ratio and subsequently added to a final 0.4 μM concentration. The samples were incubated for 10 min at RT and centrifuged for 5 min at 12,000g to remove aggregates. From the supernatant, samples were taken for native page analysis as well as MNase digestion.

For native page, glycerol was added to a final concentration of 8% and samples were run on a 6% retardation gel (Thermo Fisher Scientific) in 0.2X TBE (17.8 mM Tris, 17.8 mM Boric acid, 0.4 mM EDTA) at 150V. Gels were scanned using the ImageQuant800 imager (Amersham) for fluorescent H2B-488 signal. Subsequently gels were stained for 10 min at RT in SYBR Gold (Invitrogen) and scanned again to visualize the DNA.

MNase digestion was performed in MNase buffer (50 mM Tris pH8, 5 mM CaCl2, 0.1 mg/mL BSA) with 80 units of MNase (New England Biolabs) per reaction for 10 min at 37°C after which reactions were quenched by adding EDTA to 50 mM. Proteins were degraded by incubation with 1 unit of Proteinase K (New England Biolabs) for 20 min at 50°C. 621 bp DNA was added as loading control and DNA was purified using the MiniElute PCR purification kit (Qiagen). Purified DNA was visualized on a 6% retardation gel that was stained with SYBR Gold. In addition, the DNA fragments were analyzed and quantified using a bioanalyzer high sensitivity DNA kit (Agilent Technologies) on the Agilent bioanalyzer.

QUANTIFICATION AND STATISTICAL ANALYSIS

Statistical analysis was performed using Prism 9 (Graphpad). Statistical test used and calculated p values are indicated in the figure legends. Significance was labeled with asterisks which were defined as followed: * $p < 0.05$, ** $p < 0.01$, *** $p < 0.001$, **** $p < 0.0001$. Not significantly different samples ($p > 0.05$) were labeled with ns.

Cell Reports, Volume *42*

Supplemental information

The histone chaperone ANP32B regulates chromatin incorporation of the atypical human histone variant macroH2A

Imke K. Mandemaker, Evelyn Fessler, David Corujo, Christiane Kotthoff, Andreas Wegerer, Clément Rouillon, Marcus Buschbeck, Lucas T. Jae, Francesca Mattiroli, and Andreas G. Ladurner

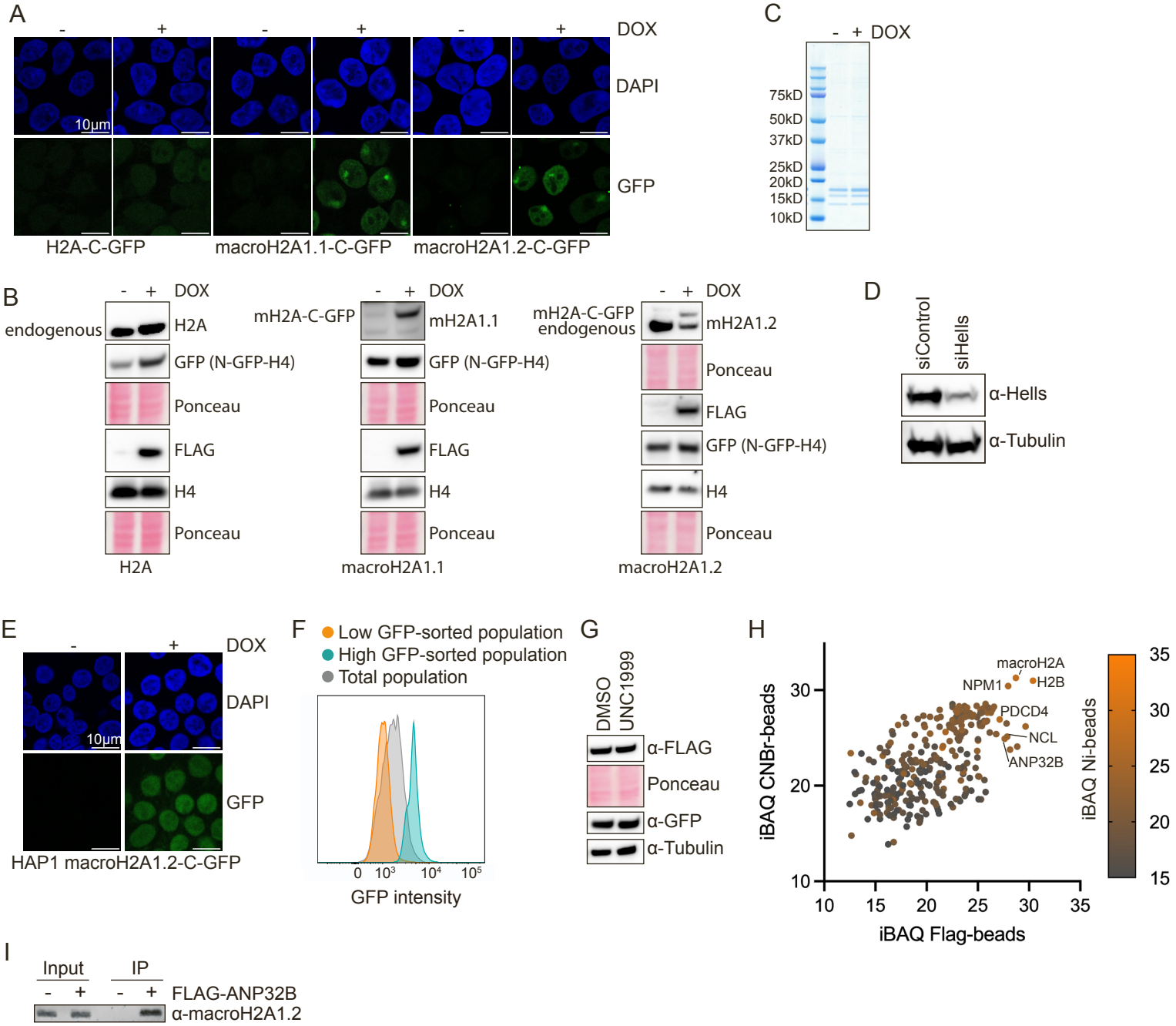
A
DOX
DAPI
GFP
10µm
H2A-C-GFP
macroH2A1.1-C-GFP
macroH2A1.2-C-GFP
C
DOX
75kD
50kD
37kD
25kD
20kD
15kD
10kD
B
DOX
endogenous
H2A
GFP (N-GFP-H4)
Ponceau
FLAG
H4
Ponceau
H2A
mH2A-C-GFP
mH2A1.1
macroH2A1.1
mH2A-C-GFP
endogenous
mH2A1.2
macroH2A1.2
D
siControl
siHells
α-Hells
α-Tubulin
E
DOX
DAPI
GFP
HAP1 macroH2A1.2-C-GFP
F
Low GFP-sorted population
High GFP-sorted population
Total population
GFP intensity
G
DMSO
UNC1999
α-FLAG
Ponceau
α-GFP
α-Tubulin
H
iBAQ CNBr-beads
iBAQ Flag-beads
iBAQ Ni-beads
macroH2A
NPM1
H2B
PDCD4
NCL
ANP32B
I
Input
IP
FLAG-ANP32B
α-macroH2A1.2
α-FLAG

Figure S1

Extended figure 1: Split-GFP-based approach to detect histone deposition as a readout for a genetic screen to identify macroH2A regulators, related to Figure 1.

A: Microscopy images of pre-extracted T-Rex split-GFP cells. Cells express GFP1-10-H4 and either H2A- Flag-GFP11, macroH2A1.1-Flag-GFP11 or macroH2A1.2-Flag-GFP11 under a doxycycline inducible promoter. Cells were fixed after 18h of DOX treatment and stained with Hoechst.

B: Western blot of T-Rex split-GFP cell lysates with or without DOX treatment. The GFP-antibody recognizes N-GFP-H4.

C: Coomassie-stained SDS-PAGE gel of low salt extracted samples from from MNase-digested macroH2A1.2 split-GFP T-Rex 293 cells.

D: Western blot showing the knock down efficiency of siHells in the macroH2A1.1 split-GFP cells. Tubulin staining is used as a loading control.

E: Microscopy images of macroH2A1.2 split-GFP HAP1 cells. Cells were pre-extracted and fixed after 18h of DOX treatment and stained with Hoechst.

F: Flow cytometry histograms showing the GFP intensities of the sorted populations in the haploid genetic screen compared to the unsorted population.

G: Western blot of DMSO or UNC1999 treated macroH2A1.2 HAP1 split-GFP cells. Tubulin and Ponceau staining are used as loading controls.

H: Intensities of proteins identified by mass spectrometry in 3 different pulldown experiments.

I: Western blot of a representative co-immunoprecipitation experiment on benzonase-treated cell extracts in which macroH2A1.2 is pulled down together with FLAG-ANP32B.

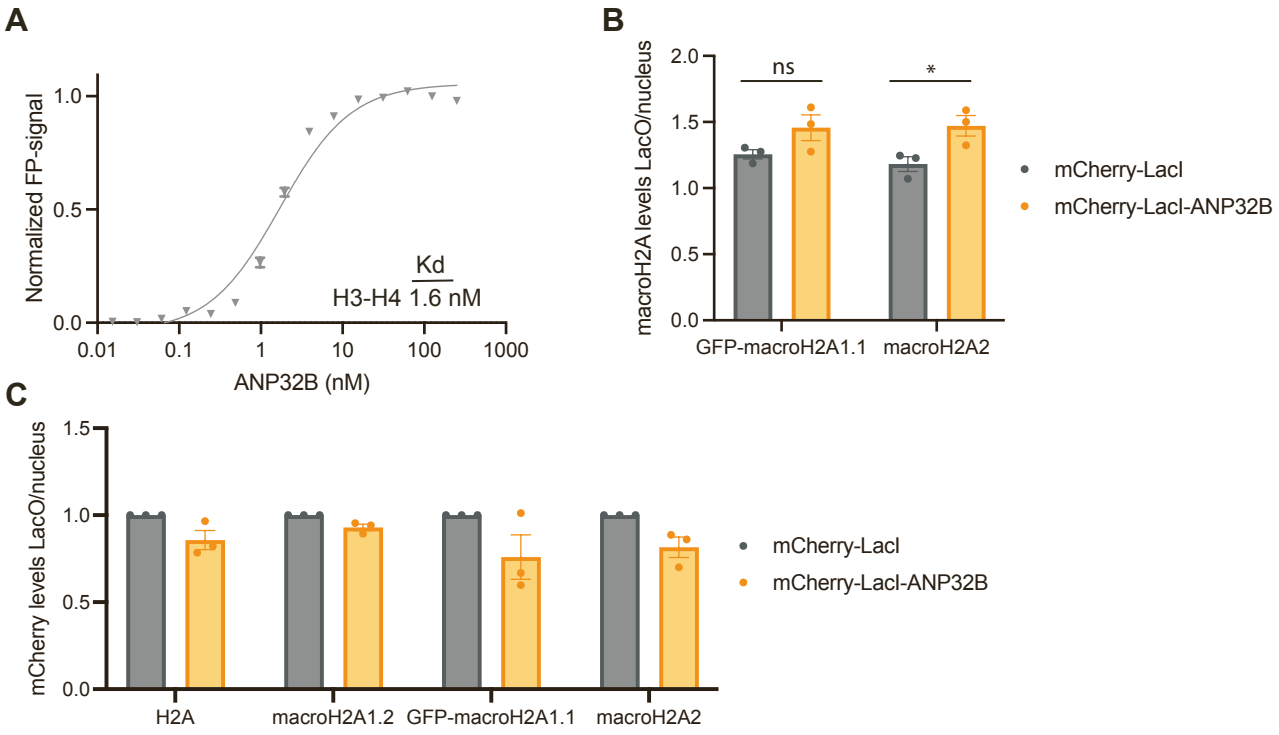
A
Normalized FP-signal
1.0
0.5
0.0
0.01
0.1
1
10
100
1000
ANP32B (nM)
Kd
H3-H4 1.6 nM
B
macroH2A levels LacO/nucleus
2.0
1.5
1.0
0.5
0.0
ns
*
GFP-macroH2A1.1
macroH2A2
mCherry-LacI
mCherry-LacI-ANP32B
C
mCherry levels LacO/nucleus
1.5
1.0
0.5
0.0
H2A
macroH2A1.2
GFP-macroH2A1.1
macroH2A2
mCherry-LacI
mCherry-LacI-ANP32B

Figure S2

Extended figure 2: ANP32B interacts with macroH2A, related to Figure 2.

A: Fluorescence polarization (FP) assay showing binding of ANP32B to Alexa-488-labeled H3-H4 tetramers. The experiment was performed in duplicate of which the average and standard deviation were plotted. A representative experiment of a total of 2 repeats is shown.

B: Quantification of LacI experiments for GFP-macroH2A1.1 and macroH2A2. The ratio of the fluorescent intensity of the histones at the LacO, as defined by the mCherry signal, over the intensity in the entire nucleus is plotted on the Y-axis. Average of three independent experiments is shown, each with at least 10 cells analyzed per condition per experiment, and error bars represent SEM. Significance is calculated using 2way-ANOVA with Šidák correction; GFP-macroH2A1.1 p=0.1522, macroH2A2 p=0.0393.

C: Quantification of mCherry intensity at the LacO/nucleus upon tethering of mCherry-LacI or mCherry-LacI-ANP32B. Average of three independent experiments is shown and error bars represent SEM. T-test with Welsh correction; H2A p=0.1216, macroH2A1.2 p=0.0633, GFP-macroH2A1.1 p=0.2001, macroH2A2 p=0.0870.

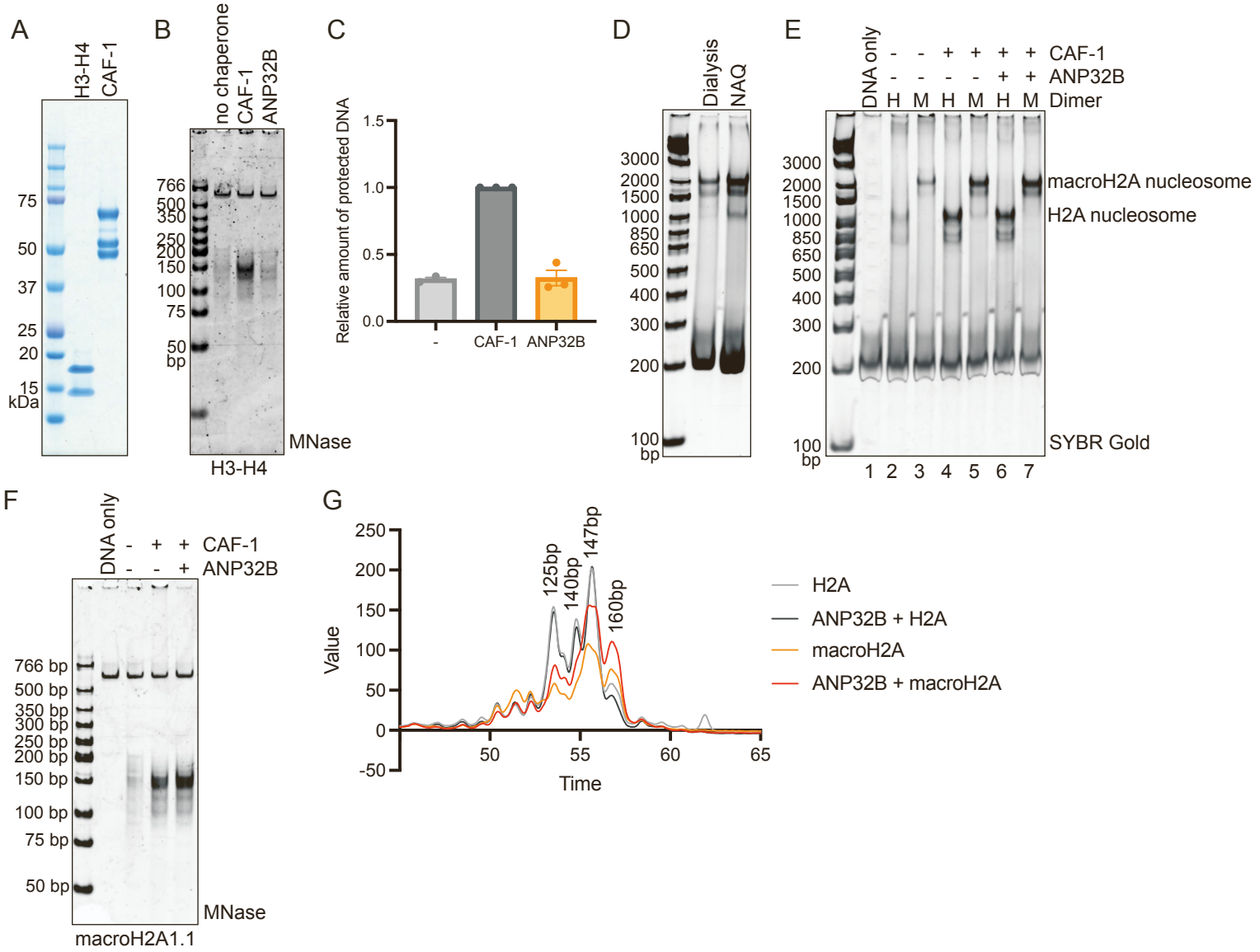
A
H3-H4
CAF-1
75
50
37
25
20
15
kDa
B
no chaperone
CAF-1
ANP32B
766
500
350
250
200
150
100
75
50
bp
MNase
H3-H4
C
Relative amount of protected DNA
1.5
1.0
0.5
0.0
-
CAF-1
ANP32B
D
Dialysis
NAQ
3000
2000
1500
1000
850
650
500
400
300
200
100
bp
E
DNA only
CAF-1
ANP32B
H M H M H M Dimer
macroH2A nucleosome
H2A nucleosome
SYBR Gold
1 2 3 4 5 6 7
F
DNA only
CAF-1
ANP32B
766 bp
500 bp
350 bp
300 bp
250 bp
200 bp
150 bp
100 bp
75 bp
50 bp
MNase
macroH2A1.1
G
125bp
140bp
147bp
160bp
Value
Time
H2A
ANP32B + H2A
macroH2A
ANP32B + macroH2A

Figure S3

Extended figure 3: ANP32B has *in vitro* macroH2A histone chaperone activity, related to Figure 3.

A: SDS-PAGE gel of recombinant human H3-H4 and Yeast CAF-1ΔKER.

B: Nucleosome assembly assay testing H3-H4 chaperone activity of yeast CAF-1ΔKER and ANP32B. Native gel shows MNase-protected DNA fragments, representing nucleosomes.

C: Quantification of nucleosomes formed when either CAF-1ΔKER or ANP32B is used as a H3-H4 chaperone. Data is normalized to +CAF-1 condition and the average and SEM of 3 independent experiments are shown. ANP32B vs no chaperone p=0.8996, as tested by two-sided T-test with Welsh correction.

D: Native gel of macroH2A-H2B nucleosomes generated with salt dialysis or in the NAQ assays. Gel is stained with SYBR Gold to visualize the DNA.

E: Native gel of NAQ assay shown in figure 4C-D stained with SYBR Gold. H=H2A-H2B and M=macroH2A-H2B.

F: Representative native PAGE of MNase-resistent DNA fragments from a macroH2A1.1 NAQ assay.

G: Bioanalyzer profile of protected DNA fragments after MNase digestion from H2A or macroH2A nucleosomes assembled with or without ANP32B.

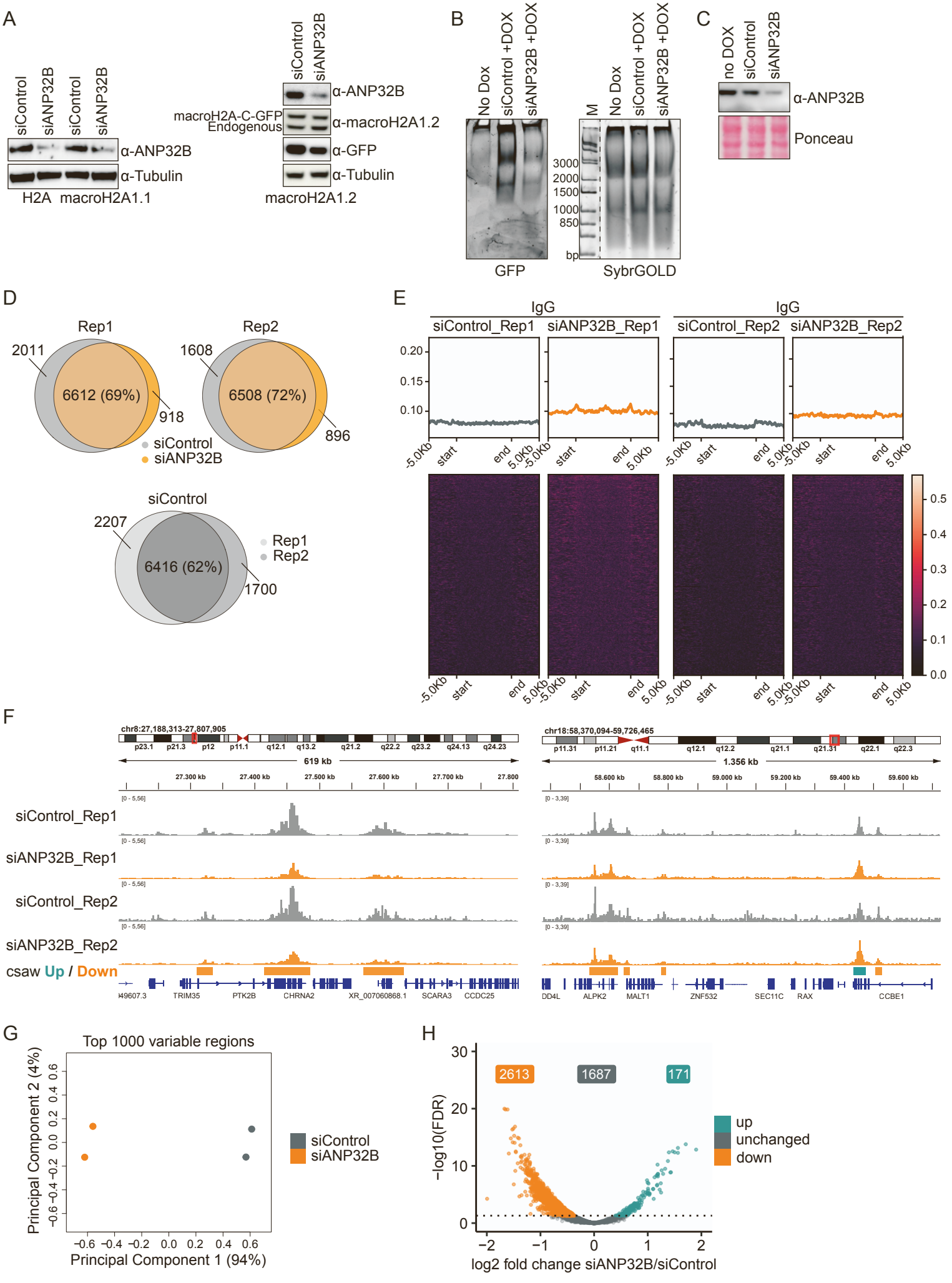
A
siControl
siANP32B
siControl
siANP32B
α-ANP32B
α-Tubulin
H2A
macroH2A1.1
siControl
siANP32B
α-ANP32B
macroH2A-C-GFP
Endogenous
α-macroH2A1.2
α-GFP
α-Tubulin
macroH2A1.2
B
No Dox
siControl +DOX
siANP32B +DOX
GFP
M
No Dox
siControl +DOX
siANP32B +DOX
3000
2000
1500
1000
850
bp
SybrGOLD
C
no DOX
siControl
siANP32B
α-ANP32B
Ponceau
D
Rep1
Rep2
2011
6612 (69%)
918
1608
6508 (72%)
896
siControl
siANP32B
siControl
2207
6416 (62%)
1700
Rep1
Rep2
E
IgG
siControl_Rep1
siANP32B_Rep1
IgG
siControl_Rep2
siANP32B_Rep2
0.20
0.15
0.10
-5.0Kb
start
end
5.0Kb
0.5
0.4
0.3
0.2
0.1
0.0
F
chr8:27,188,313-27,807,905
619 kb
chr18:58,370,094-59,726,465
1.356 kb
siControl_Rep1
siANP32B_Rep1
siControl_Rep2
siANP32B_Rep2
csaw Up / Down
TRIM35
PTK2B
CHRNA2
SCARA3
CCDC25
DD4L
ALPK2
MALT1
ZNF532
SEC11C
RAX
CCBE1
G
Top 1000 variable regions
Principal Component 2 (4%)
Principal Component 1 (94%)
siControl
siANP32B
H
2613
1687
171
−log10(FDR)
log2 fold change siANP32B/siControl
up
unchanged
down

Figure S4

Extended figure 4: ANP32B affects macroH2A deposition in cells, related to Figure 4.

A: Western blot showing siANP32B knock down efficiency in T-Rex split-GFP cell lysates. Tubulin staining is used as a loading control.

B: Native PAGE showing nucleosomes from MNase-digested macroH2A1.2 split-GFP T-REX 293 cells. GFP signal was imaged prior to SYBR Gold staining and imaging.

C: Western blot showing ANP32B depletion in the MNase experiment. Ponceau staining was used as a loading control.

D: Venn diagram showing the number of epic2 peaks identified and their overlap between the CUT&RUN samples.

E: Heatmap and mean profile visualization of the non-targeting IGG control CUT&RUN signal on the epic2 macroH2A1-enriched domains.

F: Examples of CUT&RUN signal on different genomic locations, visualized using IGV.

G: Principal component analysis plot using the window-level counts of the top 1000 most variable windows between samples as computed by csaw. The percentage of the variance explained by each principal component is in parenthesis.

H: Volcano plot of the differential binding analysis results obtained with csaw, using the combined region-level statistics by merging windows within 1kb. Regions with an FDR < 0.05 were considered differentially bound.